8

Crystallization Behavior and Control of Amorphous Alloys

Lai-Chang Zhang
The University of Western Australia
Australia

1. Introduction

Since the discovery in 1960 by Duwez (Klement et al., 1960), considerable effort has been devoted to form amorphous (or glassy) alloys either by rapid solidification techniques or by solid-state amorphization techniques (Inoue, 2000; Johnson, 1999; Suryanarayana & Inoue, 2011; Wang et al., 2004). However, the geometry of the amorphous samples has long time been limited in the form of ribbons or wires. The first "bulk" amorphous alloys, arbitrarily defined as the amorphous alloys with a dimension no less than 1 mm in all directions, was discovered by Chen and Turnbull (Chen & Turnbull, 1969) in ternary Pd-Cu-Si alloys. These ternary bulk glass-forming alloys have a critical cooling rate of about 10^2 K s^{-1} and can be obtained in amorphous state with a thickness up to 1 mm and more. Since then, especially after the presence of new bulk metallic glasses (BMGs) in $La_{55}Al_{25}Ni_{20}$ (Inoue et al., 1989) and $Zr_{41.2}Ti_{13.8}Cu_{12.5}Ni_{10.0}Be_{22.5}$ (Peker & Johnson, 1993), multicomponent BMGs, which could be prepared by direct casting from molten liquid at low cooling rates, have been drawing increasing attention in the scientific community. A great deal of effort has been devoted to developing and characterizing BMGs with a section thickness or diameter of a few millimetres to a few centimetres (Suryanarayana & Inoue, 2011). A large variety of multicomponent BMGs in a number of alloy systems, such as Pd-, Zr-, Mg-, Ln-, Ti-, Fe-, and Ni-based BMGs, have been developed via direct casting method with low cooling rates of the order of 1 – 10^2 K s^{-1} (Inoue, 2000; Johnson, 1999; Suryanarayana & Inoue, 2011; Wang, et al., 2004). In this method, the alloy compositions were carefully designed to have large glass-forming ability (GFA) so that "bulk" amorphous alloys can be formed at a low cooling rate to frustrate crystallization from molted liquid state. A number of parameters/indicators have been proposed to evaluate the GFA of multicomponent alloy systems to search for BMGs with larger dimensions (Suryanarayana & Inoue, 2011). So far, the "record" size of the BMGs is 72 mm diameter for a $Pd_{40}Cu_{30}Ni_{10}P_{20}$ bulk metallic glass (Inoue et al., 1997). The discovery of amorphous alloys has attracted widespread research interests because of their technological promise for practical applications and scientific importance in understanding glass formation and glass phenomena.

Arising from their disordered atomic structure and unique glass-to-supercooled liquid transition, amorphous alloys represent a new class of structural and functional materials with excellent properties (Eckert et al., 2007; Inoue, 2000; Johnson, 1999; Suryanarayana & Inoue, 2011; Wang, 2009; Xu et al., 2010), e.g. high strength about 2–3 times of their

crystalline counterparts, large elastic limit about 2% which is very near to some polymer materials, including extreme strength at low temperature and high flexibility at high temperature, high corrosion resistance, high wear resistance, superior chemical and physical properties, etc. These properties, which can be rarely found in crystalline materials, are attractive for the practical applications as a new class of structural and functional materials. Fig. 1 summarizes the relationship between fracture strength and Young's modulus for typical engineering materials in amorphous and crystalline states. There is a clear tendency for fracture strength to increase with increasing Young's modulus, but the slope of the linear relation corresponding to elastic elongation is significantly different between the bulk amorphous and crystalline alloys and the elastic elongation of the amorphous alloys is ~3 times larger than those for the crystalline alloys. The amorphous alloys also exhibit high strength which is ~3 times higher than those for crystalline alloys, when the comparison is made at the same Young's modulus level. Currently, amoprhous alloys have a variety of uses for sports and luxury goods, microelectromechanical systems (MEMS), biomedicine and nanotechnology.

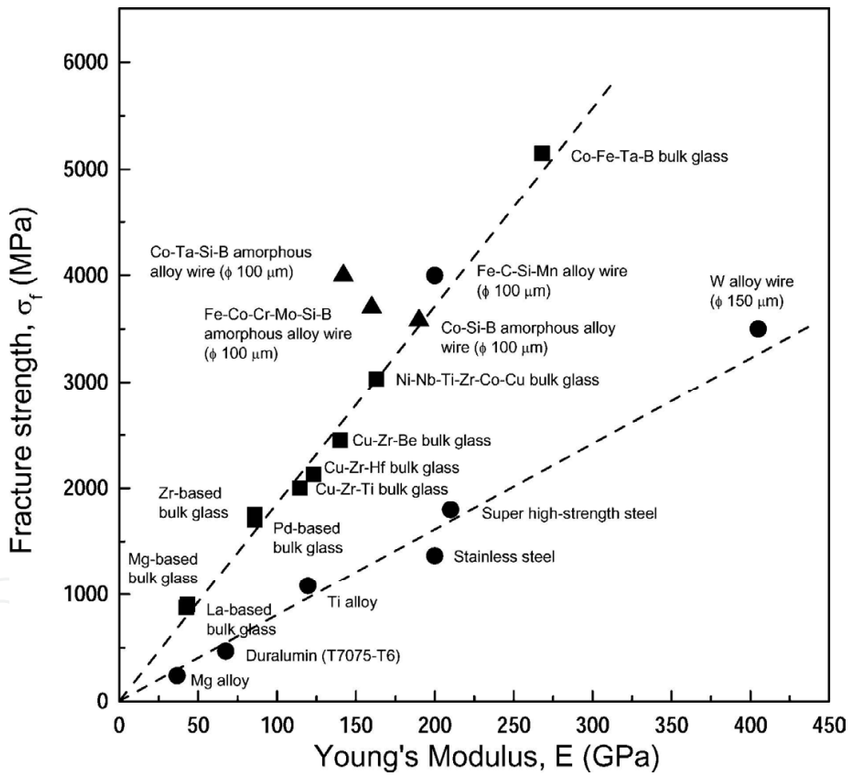

Fig. 1. Relation between strength and Young's modulus for bulk alloys in amorphous and crystalline states. Reprinted from (Inoue et al., 2004b), with permission from Elsevier.

2. Crystallization mechanisms

In general, the best practice way to describe a microstructure is in terms of its thermodynamic state before configurationally freezing set in (Turnbull, 1981). In this way, an amorphous alloy in configurationally frozen state as an undercooled liquid would be

considered metastable. By considering the local potential wells between which atoms must make diffusional jumps, even states which are thermodynamically unstable may be regarded as kinetically metastable. Such kinetic metastability can exist only where thermal activation of atomic jumps is required. Regardless of the processing route used for the formation of amorphous state, the amorphous alloys are in thermodynamically metastable state and are susceptible to transform into more stable states under appropriate circumstances. Crystallization is such a transformation during which an amorphous phase devitrified into one or more metastable or stable crystalline phases. The driving force for the crystallization is the Gibbs free energy difference between the amorphous and the crystalline states. Crystallization could happen when an amorphous solid is subject to heat treatment (Calin et al., 2007; Suryanarayana & Inoue, 2011; Zhang et al., 2002; Zhang et al., 2003; Zhang & Xu, 2004; Zhang et al., 2005a; 2005b; Zhang et al., 2006a; Zhang et al., 2007a; Zhang et al., 2007b), mechanical deformation (Fornell et al., 2010; Lohwongwatana et al., 2006; Setyawan et al., 2010), pressure (Jiang et al., 2000; Jiang et al., 2002; Jiang et al., 2003b; Yang et al., 2006; Ye & Lu, 1999), and/or irradiations (Azam et al., 1979). Amongst these processing techniques, conventionally thermal annealing is the most commonly used in the investigation on crystallization of amorphous alloys. The dimensions and morphologies of the crystallization products strongly depend on the transformation mechanism, which is closely related to the chemical composition of the amorphous phase and to the thermodynamic properties of the corresponding crystalline phase. The crystallization products could include crystalline solids (solid solution, intermetallics, and/or compounds) (Foley et al., 1997; Kelton et al., 2003; Lu, 1996; Sahu et al., 2010; Zhang, et al., 2002; Zhang, et al., 2003) or quasicrystalline (Murty et al., 2000). As the crystallization process upon annealing of an amorphous phase is much slower than during solidification of liquids, it is relatively easier to fundamentally investigate crystallization in amorphous phases than in liquids on the processes of nucleation and growth, in particular of nucleation kinetics difficult to study quantitatively in the liquid state. The study of crystallization behaviors on amorphous alloys is of primary importance not only to characterize the thermal stability of amorphous alloys against crystallization but also to investigate the fundamental aspect of the processes of nucleation and growth, which are of relevance for the understanding glass formation.

Three types of crystallization reactions that may occur during devitrification can be classified, depending on their chemical compositions (Köster & Herold, 1981; Lu, 1996): *polymorphous*, *eutectic* and *primary* crystallization. Fig. 2 shows a hypothetical free energy diagram to illustrate the crystallization reactions during crystallization. This schematic is essentially a representation of the variation of free energy with the chemical compositions of the amorphous phase and various crystalline phases (in this case, two crystalline phases, a solid solution α and a compound β, are included) at a chosen annealing temperature.

2.1 Polymorphous crystallization

In *polymorphous* crystallization, an amorphous solid crystallizes into a single crystalline phase with different structure but with same chemical composition as the amorphous phase. This reaction can only occur in concentration ranges near to those of stable compounds (C_1 in Fig. 2) or pure elements (C_2) and needs only single jumps of atoms across the crystallization front. The polymorphous crystallization reaction (reaction (1) or (2)) may produce a single compound phase (β) or a supersaturated solid solution phase (α), as shown

in Fig. 2. The crystallization mechanisms of $Fe_{33}Zr_{67}$ (Spassov & Koster, 1993), $Ni_{33}Zr_{67}$ (Lu et al., 1996), $Co_{33}Zr_{67}$ (Nicolaus et al., 1992) and $Zr_{50}Co_{50}$ (Köster & Meinhardt, 1994) amorphous alloys are the typical polymorphous crystallization.

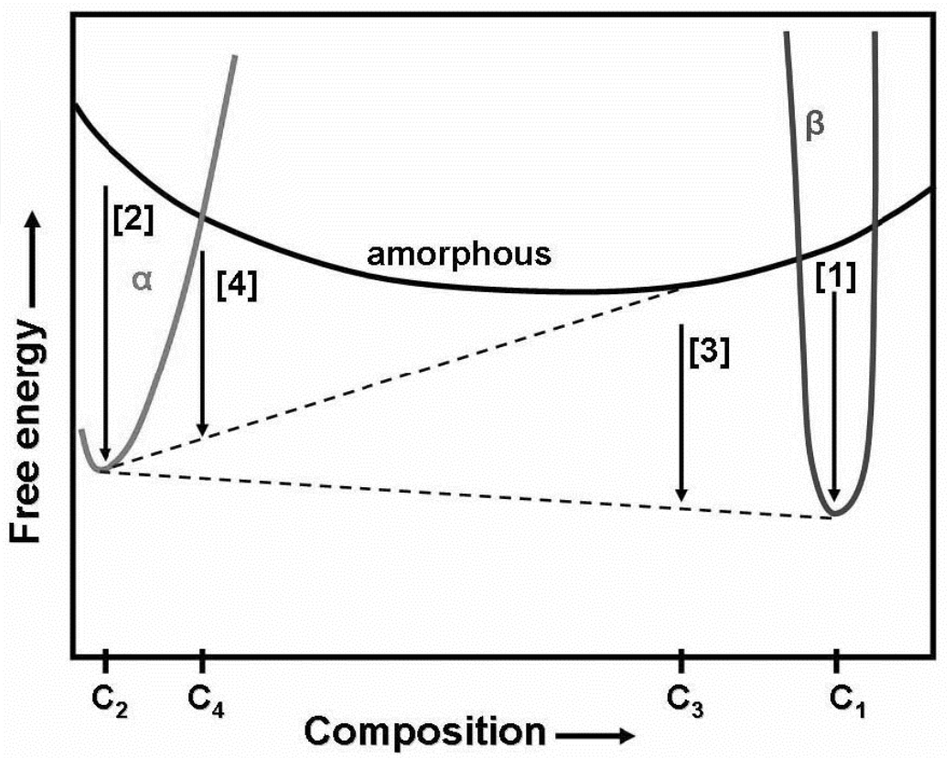

Fig. 2. Hypothetical free energy diagram to illustrate the crystallization of amorphous alloys. Reprinted from (Lu, 1996), with permission from Elsevier.

2.2 Eutectic crystallization

In case of *eutectic* crystallization, amorphous phase crystallizes into two crystalline phases simultaneously (e.g. reaction (3) in Fig. 2, α + β), during which two phases grow in a coupled fashion. This is similar to the eutectic crystallization of liquids. The reaction has the largest driving force and the overall composition of the two phases remains the same as that of the amorphous matrix. The eutectic crystallization can occur within a concentration range around the equilibrium eutectic composition rather than a specific eutectic composition as observed in conventional crystallization. A possible reason might be that the crystalline material contains a large amount of interface that may have higher energetic configurations and thus allows a relatively wide composition range (Lu, 1996). For example, e.g. in the Ni-P binary system eutectic crystallization occurs within 18.2–20.0 at.% P (i.e. amorphous → Ni + Ni_3P), where the equilibrium eutectic composition is 19.0 at.% (Dong et al., 1994).

2.3 Primary crystallization

In *primary* crystallization, amorphous phase crystallizes into a phase with different composition (C_4 in Fig. 2) in the first step (this can be either a supersaturated solid solution

or an intermetallic compound) embedded in an amorphous matrix (amorphous phase (C_4) = α + amorphous phase' (C_3)). During this reaction, a concentration gradient occurs at the interface between the precipitate and the matrix until the reaction reaches the metastable equilibrium. The residual amorphous phase (with the new concentration C_3) crystallizes, in the second step, into crystalline phases through the mechanism of either the *eutectic* or *polymorphous* crystallization. The crystallization mechanisms of most of Al-based, e.g. $Al_{88}Ni_4Y_8$ (Jiang et al., 1997), and Fe-based amorphous alloys, e.g. $Fe_{73.5}Si_{13.5}B_9Nb_3Cu_1$ (Finemet) (Hono et al., 1992), are typically primary crystallization (Foley, et al., 1997; Kelton, et al., 2003). The control of primary crystallization behaviors could lead to nanocrytalline–amorphous composites with special mechanical or functional properties (see *Section 5.1*).

3. Influences on crystallization of amorphous alloys

The mechanisms and products of crystallization of amorphous alloys are influenced by both inherent (e.g. composition, oxygen) and extraneous (e.g. preparation method, pressure, etc) factors.

3.1 Effect of chemical composition

During the searching for strong glass-forming alloys, the effect of composition on the crystallization behavior has been extensively studied in a variety of amorphous alloys, despite of the preparation methods (Suryanarayana & Inoue, 2011). Two examples are listed in this section to show how the chemical compositions of amorphous alloys influence the crystallization mechanism and crystallization products.

Zhang et al. (Zhang, et al., 2002) has investigated the addition of Al on the glass formation and crystalliztion in the ball-milled amorphous $Ti_{50}(Cu_{0.45}Ni_{0.55})_{44-x}Al_xSi_4B_2$ (x=0, 4, 8 and 12) alloys. Al additions were introduced to simultaneously replace part of the Cu and Ni in $Ti_{50}Cu_{20}Ni_{24}Si_4B_2$ (Zhang & Xu, 2002) to further reduce the density of the resulting alloys and improve the thermal stability of the supercooled liquid. The Ti-based amorphous alloy powders prepared through this solid-state process exhibit a well-defined glass transition and a supercooled liquid region. Al addition has changed the crystallization mechanims and crystallizaiton products of the amoprhous $Ti_{50}Cu_{20}Ni_{24}Si_4B_2$ alloy. Fig. 3 (a) displays the differential scanning calorimetry (DSC) scans for the as-milled samples with different Al contents. In all cases, an endothermic signal associated with the glass transition is evident. As see from Fig. 3 (a), the onset of glass transition temperature (T_g) is apparently insensitive to the change in the overall alloy composition. With increasing Al substitution, the exothermic reaction due to crystallization occurs at higher temperatures and the single-step crystallization event changes to a two-step process. X-ray diffraction (XRD) has been used to identify the structural changes associated with the exothermal events at several different temperatures, as marked by dots in the DSC traces in Fig. 3 (b). For x = 0, the XRD pattern at 777 K crystallization peak and after the crystallization event (810 K) showed that the amorphous phase transformed into the cubic NiTi phase and an unknown phase. The same products were found for x = 4 after crystallization, as shown in the XRD pattern at 820 K. Such a transition can be regarded as a eutectic crystallization, by which the amorphous phase simultaneously transforms into more than two phases in one step (as stated in *Section 2.2*). For x = 8 and x = 12, on the other hand, crystallization is completed in two steps. Fig. 3

(b) indicates that in addition to the NiTi phase precipitated in the first stage of the crystallization, the second crystallization peak in the DSC traces arises from the appearance of the Ti_2Ni intermetallic compounds in the final crystallization products.

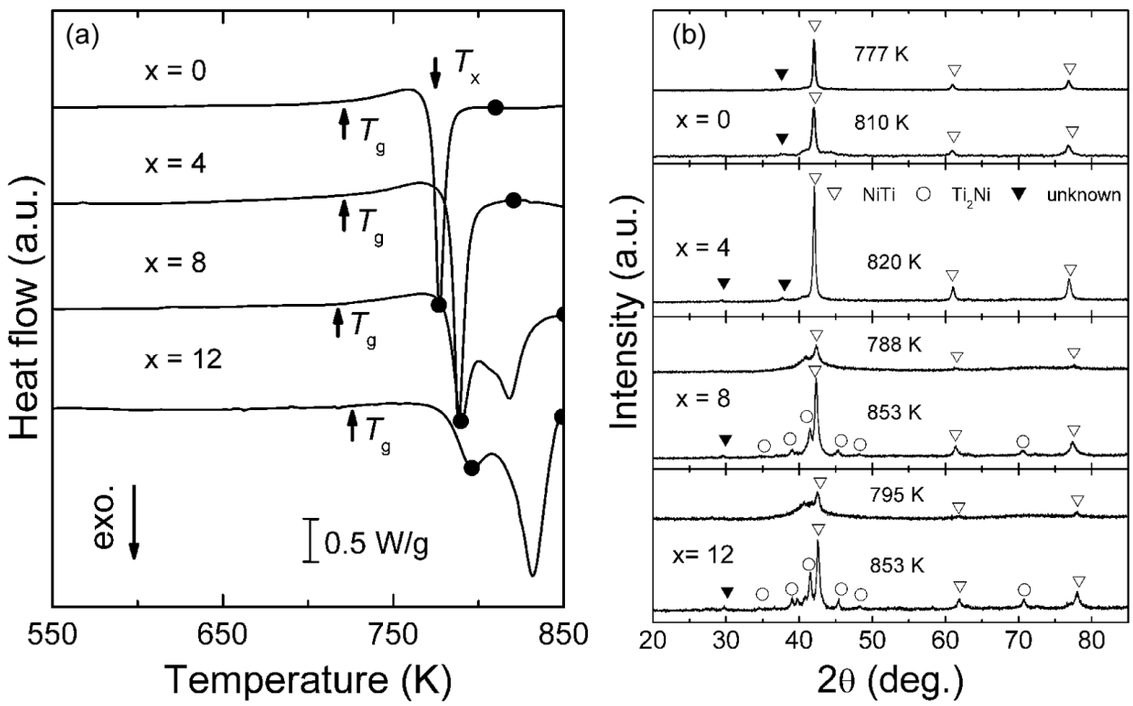

Fig. 3. (a) DSC scans and (b) the corresponding XRD patterns measured at room temperature after heating to different temperatures in DSC at a heating rate of 40 K/min for the mechanically alloyed $Ti_{50}(Cu_{0.45}Ni_{0.55})_{44-x}Al_xSi_4B_2$ (x=0, 4, 8, 12) powders. Reprinted from (Zhang, et al., 2002), with permission from Cambridge University Press.

The glass formation and crystallization behavior in multicomponent Zr-based alloys have been intensively investigated. In general, multicomponent Zr-based alloys can be used for the production of fully amorphous bulk samples with dimensions up to centimeter order, or for the formation of bulk nanostructured materials. However, the phase selection upon crystallization is strongly affected by the chemical composition of the amorphous phase. In order to obtain nanostructured materials from amorphous precursors (see *Section 5.1*), amorphous specimens are typically annealed at temperatures within the supercooled liquid region (the temperature region between onset glass transition temperature, T_g, and the onset of crystallization, T_x,) or close to T_x. Eckert et al (Eckert et al., 2001) has investigate the crystallization behaviors of Zr-based BMGs and produce bulk nanostructured alloys by partial crystallization of the Zr-based BMGs precursors. Fig. 4 (a) displays the DSC scans for as-cast $Zr_{62-x}Ti_xCu_{20}Al_{10}Ni_8$ glassy alloys (x = 0, 3, 5, and 7.5). $Zr_{62}Cu_{20}Al_{10}Ni_8$ crystallizes via one sharp exothermic peak to form several intermetallic compounds. Upon Ti addition, the crystallization mode changes toward a double-step process. With increasing Ti content, the first DSC peak shifts to lower temperatures and the enthalpy related to the second exothermic peak decreases. The samples were isothermally annealed for different times below T_x for further study of the crystallization process. The crystallization products after

annealing were investigated by XRD (Fig. 4(b)). $Zr_{62}Cu_{20}Al_{10}Ni_8$ transforms into cubic $NiZr_2$-type and tetragonal CuZr2-type compounds. Annealing the alloy with x = 3 leads to primary precipitation of an icosahedral quasicrystalline (QC) phase with spherical morphology and a size of about 50 to 100 nm. For x = 5, the diffraction peaks are weaker in intensity and broader because the precipitates are as small as about 5 nm. For x = 7.5, the precipitates are about 3 nm in size. At first glance the XRD pattern (Fig. 4 (b)) after annealing displays no obvious reflections but only broad amorphous-like maxima. However, careful examinations of the annealed state by high intensity synchrotron radiation and/or by transmission electron microscopy (TEM) (Eckert, et al., 2001) clearly shows differences in scattering intensity compared to the as-cast state indicates the precipitation of a metastable cubic phase with a grain size of ~2 nm coexisting with a residual amorphous phase.

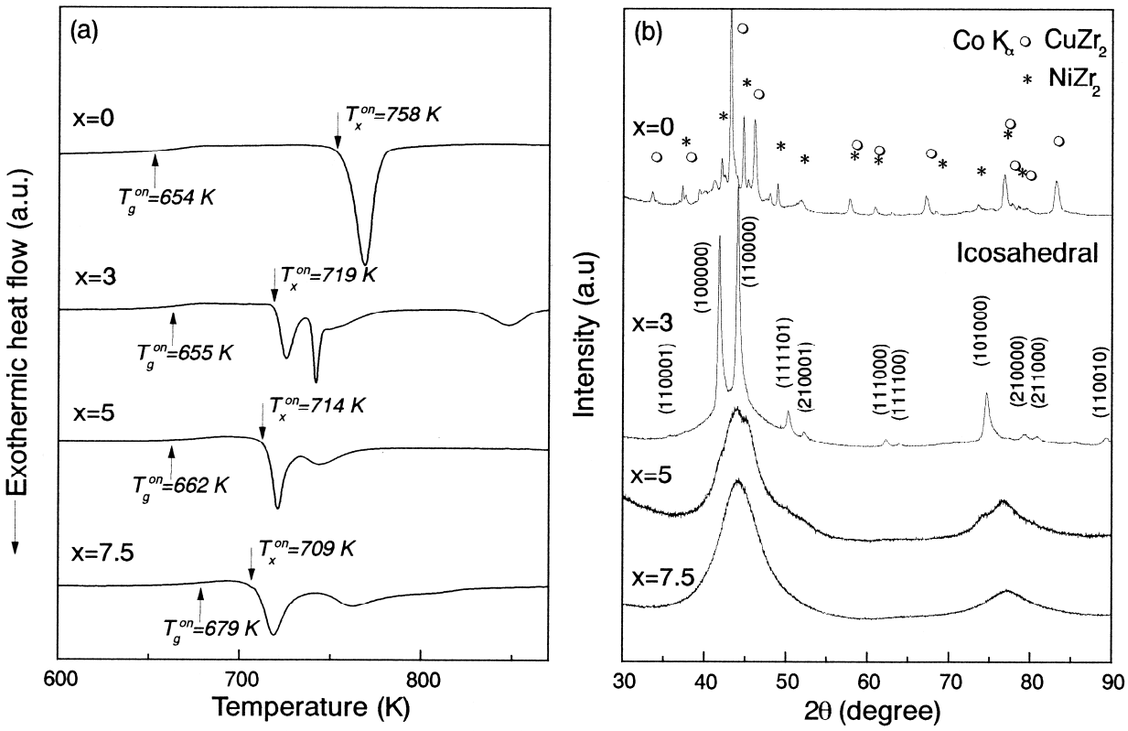

Fig. 4. (a) DSC scans and (b) corresponding XRD patterns after isothermal annealing for the $Zr_{62-x}Ti_xCu_{20}Al_{10}Ni_8$ (x = 0, 3, 5, and 7.5) amorphous alloys: x = 0, annealed at 723 K for 30 min; x = 3, annealed at 703 K for 5 min; x = 5, annealed at 683 K for 30 min and x = 7.5 annealed at 688 K for 40 min. Reprinted from (Eckert, et al., 2001), with permission from Elsevier.

3.2 Effect of oxygen

Although Zr-based BMGs have shown high glass-forming ability, high thermal stability and excellent mechanical properties, the glass-forming ability of these BMGs appears to be significantly affected by the contamination of oxygen either from the raw materials or from the processing (Inoue et al., 1995a; Kubler et al., 1998; Lin et al., 1997). The investigation of the influence of oxygen on the crystallization behavior of Zr-based amorphous alloys

(Altounian et al., 1987) showed that the oxygen induces the formation of metastable face-centered cubic (fcc) $NiZr_2$, thereby reducing the thermal stability of the Zr-Ni amorphous alloys. Extensive studies have proved that oxygen enhances the crystallization reaction in Zr-based amorphous alloys. For example, Lin et al (Lin, et al., 1997) reported for undercooled Zr–Ti–Cu–Ni–Al molten liquids that oxygen addition strongly affects crystal nucleation and can dramatically increase the necessary critical cooling rate for glass formation, thus limiting bulk glass formation and reducing the maximum attainable sample thickness. Over the range of oxygen content studied (300 – 5000 at. ppm), the time–temperature-transformation curves vary roughly by two orders of magnitude along the time axis. In other words, oxygen contamination ranging up to 0.5 at.% can increase the necessary cooling rate for glass formation by two orders of magnitude (Lin, et al., 1997). Köster et al. (Köster et al., 1996; Köster et al., 1997) reported the formation of an icosahedral phase during primary crystallization in $Zr_{65}Cu_{17.5}Ni_{10}Al_{7.5}$ amorphous alloys, whereas such a crystallization process was not reported in the same alloy composition by Zhang et al. (Zhang et al., 1991), indicating that the formation of quasicrystals is induced by the oxygen contamination in the alloy. Eckert and his co-workers (Eckert et al., 1998; Gebert et al., 1998) also reported the strong influence of the oxygen contamination on the crystallization kinetics and products in $Zr_{65}Cu_{17.5}Ni_{10}Al_{7.5}$ amorphous alloy, where supercooled liquid region decreases with increasing oxygen content due to the change in crystallization sequence from a single- to a double-step process. It was also shown that an fcc $NiZr_2$ phase is formed at a higher oxygen level in the Zr–Cu–Ni–Al system. Therefore, oxygen contamination is of primary importance for the glass formation and crystallization behavior of Zr-based amorphous alloys.

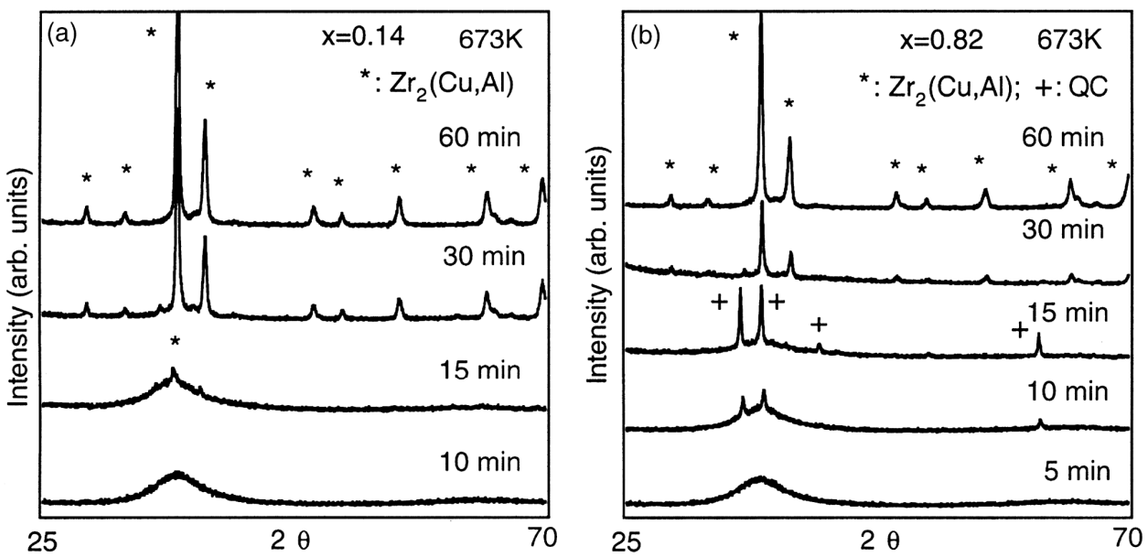

Fig. 5. XRD patterns of the $Zr_{65-x}Cu_{27.5}Al_{7.5}O_x$ bulk amorphous alloys with (a) x = 0.14 and (b) x = 0.82 after annealing at 673 K for different durations. Reprinted from (Murty, et al., 2000), with permission from Elsevier.

Murty et al. (Murty, et al., 2000) investigated the influence of oxygen on the crystallization behavior of melt-spun amorphous $Zr_{65-x}Cu_{27.5}Al_{7.5}O_x$ (x = 0.14, 0.43 and 0.82) ribbons. DSC

results showed that the T_g increases with the addition of oxygen. The base alloy containing the lowest amount of oxygen (x = 0.14) crystallizes in a single step. The addition of oxygen significantly decreases the width of supercooled liquid region (ΔT_x) from 85 K for x = 0.14 to 58 K for x = 0.82. The decrease in ΔT_x is partly due to the increase in T_g with increasing oxygen and also due to the appearance of a pre-crystallization peak in the oxygen-containing alloys before the main crystallization event. The base alloy heated to 673 K (in supercooled liquid region) shows an amorphous nature. In the x = 0.82 alloy, precipitation of spherical icosahedral particles in nanocrystalline state was observed within 10 min annealing at 673 K. Then it crystallizes to Zr_2(Cu,Al) when heated to 723 K. No other phase is present in the alloy heated up to 753 K. The x = 0.82 alloy heated to 673 K has a similar trend to that of the base alloy. However, the alloy heated near the pre-crystallization peak (708 K) led to the presence of an icosahedral phase along with a small amount of Zr_2(Cu,Al). Only Zr_2(Cu,Al) is present in the alloy heated to 723 and 753 K. The base alloy with x = 0.14 remains amorphous for up to 10 min at 673 K, after which the formation of Zr_2(Cu,Al) was observed. The XRD patterns in Fig. 5 (a) clearly indicate the formation of Zr_2(Cu,Al) beyond 10 min of annealing at 673 K. No other phase was identified even after a longer annealing for 60 min (Fig. 5 (a)). XRD patterns of the alloy heat treated at 673 K (Fig. 5 (b)) show that the icosahedral phase starts forming after 10 min and persists for up to 15 min, beyond which the icosahedral phase transforms to Zr_2(Cu,Al).

The mechanism of the oxygen-induced precipitation of metastable fcc Zr_2(Cu,Al) and icosahedral quasicrystalline phases is rationalized by considering the effect of oxygen on the nucleation process. The high thermal stability of multicomponent Zr-based amorphous alloys is generally attributed to the difficulty of precipitation of crystalline compounds from the undercooled liquid. The combination of elements with significantly different atomic sizes and negative enthalpies of mixing leads to a homogeneously mixed dense random packed structure of the liquid resulting in a large liquid–solid interface energy (Inoue, 2000). If the nucleating phase has a different composition with respect to the homogeneous undercooled liquid, then the nucleation of the phase requires substantial atomic rearrangement (Eckert, et al., 1998). The driving force for the polymorphous crystallization is ΔG_{total}. However, if the icosahedral phase is stabilized by oxygen addition, the driving force for the primary crystallization of the icosahedral phase can be comparable to or higher than that for the polymorphous crystallization, ΔG_{total}. In such a case, icosahedral phase would initially precipitate from the amorphous matrix by the primary crystallization. The free energy reduction is accompanied with this crystallization and there is still a driving force to form Zr_2(Cu,Al) from the icosahedral phase and/or the remaining amorphous phase in the second stage. The formation of the icosahedral phase would be preferable if the driving forces for the polymorphous crystallization and the primary crystallization are comparable, because it is believed that icosahedral clusters are present in the amorphous phase, and these would act as nuclei for the icosahedral phase primary crystals. If such icosahedral clusters are stabilized by the presence of oxygen, the oxygen-enriched alloy would be favour to form an icosahedral phase by primary crystallization. The differences in the sequence of the phase formation in these alloys with x = 0.14 and 0.82 are illustrated schematically in Fig. 6, in which the darkness of the gray scale corresponds to the concentration of Zr. In the base Zr–Cu–Al and Zr–Cu amorphous alloys, crystallization proceeds by polymorphous reaction without change in composition. On the other hand, in the oxygen-containing ternary alloys, the first stage of crystallization occurs by primary

crystallization of the icosahedral phase. The icosahedral phase is enriched in Zr and O and depleted in Cu and Al. When Zr_2(Cu,Al) precipitates peritectically, the concentration of the Zr_2(Cu,Al) particles becomes the same as the initial alloy composition. When this reaction is complete, only the grains of single-phase Zr_2(Cu,Al) remain.

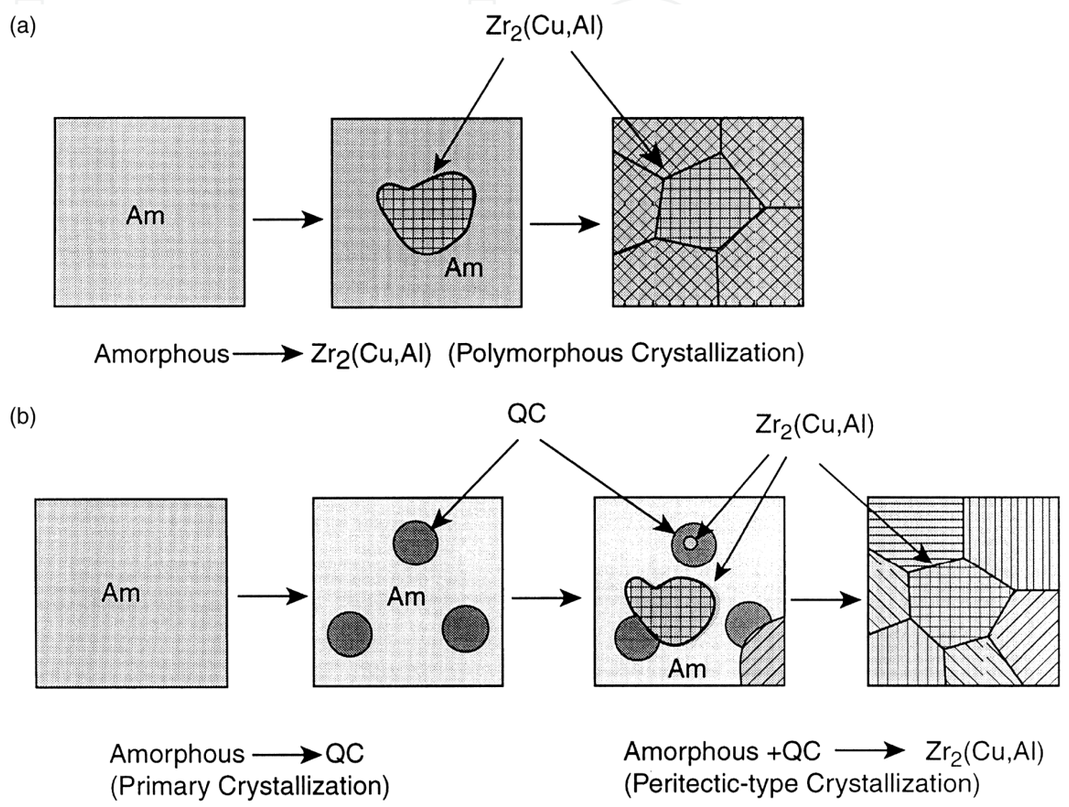

Fig. 6. Schematic diagrams showing the evolution of microstructure during crystallization of $Zr_{65-x}Cu_{27.5}Al_{7.5}O_x$ amorphous with (a) x = 0.14 and (b) x = 0.82. Reprinted from (Murty, et al., 2000), with permission from Elsevier.

3.3 Effect of sample preparation method

In general, when the transformation temperatures (e.g. T_g and T_x, etc) of an amorphous alloy are measured by DSC, there is no appreciable difference between in the amorphous samples prepared by direct melt cooling from molten liquid (e.g. by melt spinning, casting, water quenching, etc). Table 1 summarizes the transformation temperatures determined from DSC for some typical amorphous alloys prepared by different routes. Furthermore, there is no difference in the transformation temperatures of the amorphous rods with different sizes. As seen from Table 1, same transformation temperatures are obtained in the $Mg_{65}Cu_{15}Y_{10}Ag_{10}$ amorphous rods in 6 mm diameter prepared by injection casting and in 10 mm diameter prepared by squeeze casting.

Composition	Synthesis route	T_g (K)	T_x (K)	ΔT_x (K)	Reference
$Cu_{50}Zr_{50}$	Cu-mold casting	675	732	57	(Inoue et al., 2005)
	Melt spinning	686	744	58	
$Cu_{60}Zr_{30}Ti_{10}$	Cu-mold casting (2.5 mm∅ rod)	714	758	44	(Jiang et al., 2003a)
	Melt spinning	711	754	43	
$Pd_{40}Ni_{40}P_{20}$ (fluxed)†	Water quenching (7 mm∅ rod)	576	678	102	(He et al., 1996)
	Melt spinning	590	671	91	(Inoue, et al., 1997)
$Pd_{81}Si_{19}$ (fluxed)†	Air cooling	638	696	58	(Yao & Ruan, 2005)
	Melt spinning	633	675	42	
$Mg_{65}Cu_{15}Y_{10}Ag_{10}$	Melt spinning	428	469	41	(Kang et al., 2000)
	Injection casting (6 mm∅ rod)	428	469	41	
	Squeeze casting (10 mm∅ rod)	428	469	41	
$Pd_{40}Cu_{30}Ni_{10}P_{20}$ (fluxed)	Melt spinning	572	670	98	(Inoue, et al., 1997)
$Pd_{40}Cu_{30}Ni_{10}P_{20}$ (unfluxed)	Melt spinning	572	663	91	
$Zr_{65}Al_{7.5}Ni_{10}Cu_{17.5}$	Water quenching (16 mm∅ rod)	625	750	125	(Inoue et al., 1993b)
	Melt spinning	622	749	127	
$Zr_{55}Ni_{25}Al_{20}$	Planar flow casting (30 μm thick ribbon)	805	820	15	(Illeková et al., 1997)
	Water quenching (9 mm∅ rod)	738	795	57	
$La_{55}Al_{25}Ni_{10}Cu_{10}$	High-pressure die casting (9 mm∅ rod)	460	527	67	(Inoue et al., 1993a)
	Melt spinning	480	550	90	
$Ti_{50}Cu_{35}Ni_{12}Sn_3$	Ball Milling	652	717	65	(Zhang, et al., 2005a)
	Melt spinning	675	739	64	
$Ti_{50}Cu_{18}Ni_{22}Al_4Sn_6$	Ball Milling	705	771	66	(Zhang, et al., 2005a)
	Melt spinning	721	789	68	

† heating rate is 0.33 K/s.

Table 1. Comparison of the transformation temperatures determined from DSC at heating rate is at 0.67 K/s (if not indicated) for some typical amorphous alloys prepared by different methods. T_g: glass transition temperature; T_x: onset crystallization temperature; ΔT_x: the width of supercooled liquid region, which is equal to $T_x - T_g$.

Fig. 7 compares the DSC curves for the $[(Fe_{0.8}Co_{0.2})_{0.75}B_{0.2}Si_{0.05}]_{96}Nb_4$ bulk amorphous alloy rods with different diameters up to 2.5 mm with the data for melt-spun ribbon of the same composition. No appreciable difference is recognized in the transformation temperatures or

crystallization process between the melt-spun ribbon and cast rod samples, in spite of an increase in Curie temperature (T_c) with the increase of diameter. All samples exhibit a distinct glass transition at 830 K, followed by crystallization at 880 K, resulting in a large supercooled liquid region of 50 K. Similar results have been obtained in a number of bulk glass-forming alloy systems (Suryanarayana & Inoue, 2011).

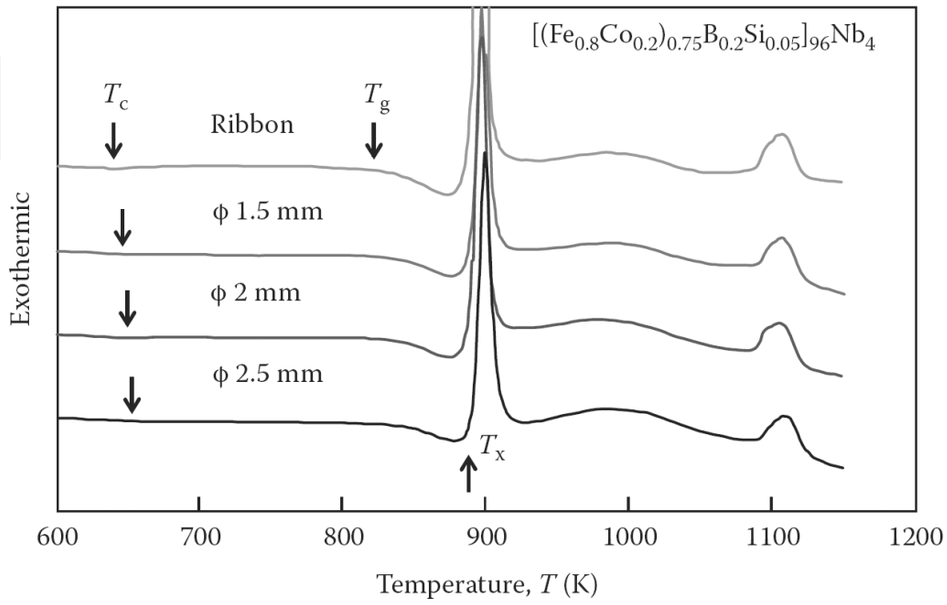

Fig. 7. DSC curves at a heating of 0.67 K/s for $[(Fe_{0.8}Co_{0.2})_{0.75}B_{0.2}Si_{0.05}]_{96}Nb_4$ bulk amorphous alloy rods (1.5, 2 and 2.5 mm∅) as well as the melt-spun amorphous alloy ribbon of the same composition. Reprinted from (Inoue et al., 2004a) and (Suryanarayana & Inoue, 2011), with permission from Elsevier.

Note that, although no appreciable difference in transformation temperatures has been observed in the amorphous alloys prepared by direct melt cooling from molten liquid, some alloys do have shown some differences in the transformation temperatures in the amorphous ribbon and rod samples, even though they have an identical chemical composition. As seen from Table 1, the $Zr_{55}Ni_{25}Al_{20}$ glassy alloys prepared by two different solidification methods (one is planar flow casting with cooling rate of about 10^5 K s^{-1} and the other is water quenching with a solidification rate of about 10^2 K s^{-1}) showed a significant difference in the transformation temperatures, i.e. 69 K difference in T_g and 15 K in T_x (Illeková, et al., 1997). By comparing the enthalpy of structural relaxation in DSC curves and the full width at half maximum (FWHM) of the first diffuse peak in XRD patterns, it is concluded that the samples produced from both methods represent the same amorphous state, but the amorphous ribbon sample contains a higher degree of short-range order (SRO) (Illeková, et al., 1997).

A number of investigations have reported a distinct difference in the transformation temperatures between the amorphous alloys prepared by melt cooling and that formed by solid-state amorphization techniques (e.g. ball milling or mechanical alloying). Fig. 8 compares the structural feature and transformation temperatures for $Ti_{50}Cu_{35}Ni_{12}Sn_3$ and

$Ti_{50}Cu_{18}Ni_{22}Al_4Sn_6$ alloys prepard by ball-milling (BM) and melt-spinning (MS). The broad diffuse maximum for the amorphous phase formed by BM is determined to be 26.89 nm^{-1} for $Ti_{50}Cu_{35}Ni_{12}Sn_3$ and 26.64 nm^{-1} for $Ti_{50}Cu_{18}Ni_{22}Al_4Sn_6$, respectively. They are well in agreement with the values of the amorphous alloys prepared using MS method, Q_p = 26.81 nm^{-1} for $Ti_{50}Cu_{35}Ni_{12}Sn_3$ and 26.67 nm^{-1} for $Ti_{50}Cu_{18}Ni_{22}Al_4Sn_6$, respectively. It implies that for a given alloy, the amorphous phase obtained using the different preparation methods is very similar in the all cases. However, both T_g and T_x of the BM alloy shift towards a lower temperature, with respect to the MS alloys, by about 20 K for $Ti_{50}Cu_{35}Ni_{12}Sn_3$ and 16-18 K for $Ti_{50}Cu_{18}Ni_{22}Al_4Sn_6$, respectively, even though a very close ΔT_x is obtained in the BM and MS amorphous alloys for each phases. Furthermore, the heat of crystallization in the BM amophous state is slightly lower than that in MS one for both alloys. The difference in the transformation temperaturees betwen the BM and MS amorphous phase is likely caused by the minor difference in the composition, oxygen content, and/or short-range order in the amorphous phases formed by different processing route.

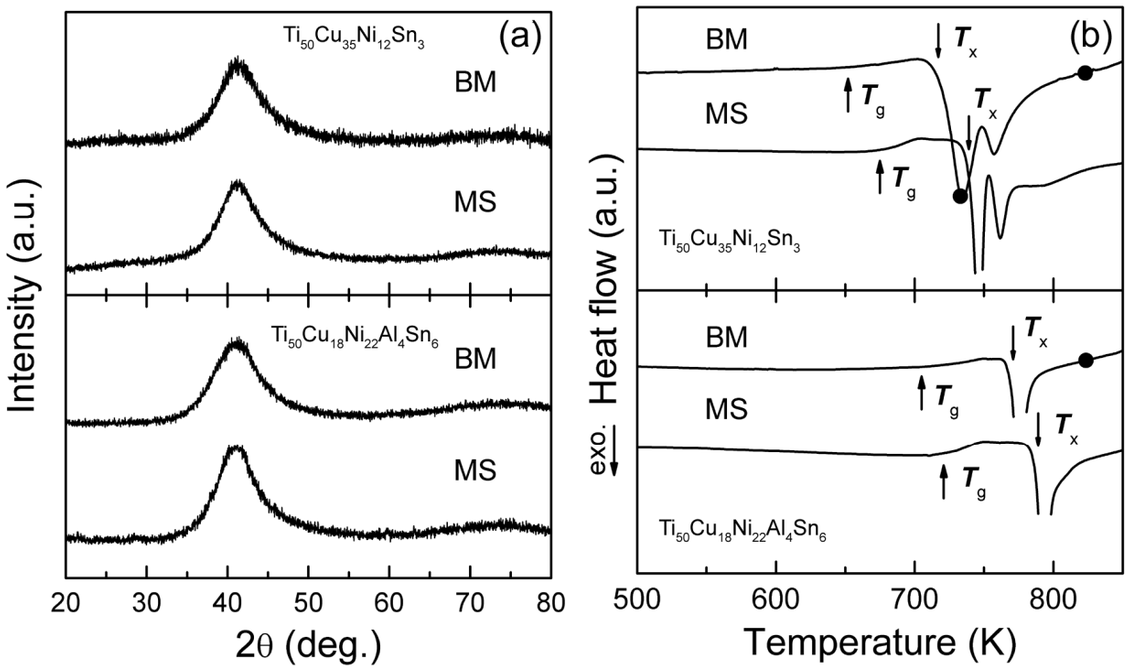

Fig. 8. (a) XRD patterns and (b) DSC curves at a heating of 0.67 K/s for $Ti_{50}Cu_{35}Ni_{12}Sn_3$ and $Ti_{50}Cu_{18}Ni_{22}Al_4Sn_6$ alloys prepard by ball-milling (BM) and melt-spinning (MS). Reprinted from (Zhang, et al., 2005a), with permission from Elsevier.

3.4 Effect of pressure

A few work has investigated the effect of high pressure on the crystallization of amorphous alloys, e.g. see the references (Jiang, et al., 2000; Jiang, et al., 2002; Jiang, et al., 2003b; Ye & Lu, 1999; Zhuang et al., 2000). In general, the crystallization temperature of an amorphous alloy increases with increasing pressure. However, the rate and the range of such temperature increase are closely related to the alloy systems. Fig. 9 shows the pressure dependence of the crystallization temperatures (i.e. T_{x1} and T_{x2}) for the $Al_{89}La_6Ni_5$

amorphous alloy. Both T_{x1} and T_{x2} firstly decrease with the increase in pressure in the range of 0–1 GPa and then increase with pressure increasing up to 4 GPa. Such changes in crystallization temperature with pressure is related to the competing process between the thermodynamic potential barrier and the diffusion activation energy under pressure (Zhuang, et al., 2000).

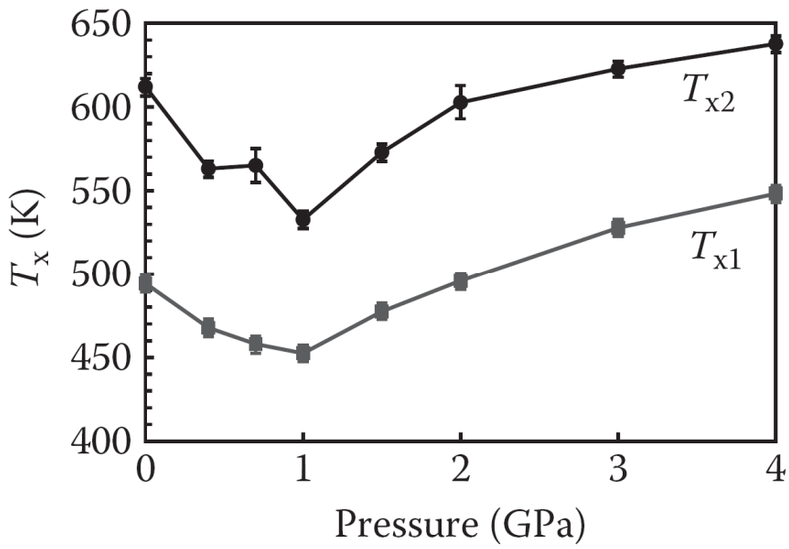

Fig. 9. Pressure dependence of the crystallization temperatures for $Al_{89}La_6Ni_5$ amorphous alloy. Reprinted from (Zhuang, et al., 2000), with permission from American Institute of Physics.

Crystallization of an amorphous alloy is normally regarded as a process proceeding by nucleation and subsequent growth of crystals. During the initial stage of nucleation of crystals in the amorphous phase, the effect of pressure on the crystallization kinetics is associated with the atomic diffusion process and the volume change effect. The crystallization temperature(s) of an amorphous alloy may be governed by the thermodynamic potential barrier of nucleation and diffusion activation energy. According to crystallization kinetics theory, the nucleation rate I can be written as,

$$I = I_0 \exp[-(\Delta G^* + Q_n) / kT] \quad (1)$$

where I_0 is a constant, ΔG^* is the free energy required to form a nucleus of the critical size, i.e., the thermodynamic potential barrier of nucleation, Q_n is the activation energy for the transport of an atom across the interface of an embryo, and k is the Boltzmann's constant. The sum $\Delta G^* + Q_n$ is called the nucleation work.

In the $Al_{89}La_6Ni_5$ alloy, ΔG^* is much larger than Q_n and the dominant factor at low pressures (0–1 GPa). Thus, the nucleation work decreases with increasing pressure, leading to an enhancement of nucleation rate I and a reduction of the crystallization temperature with increasing pressure, as shown in Fig. 9. With increasing pressure, ΔG^* rapidly decreases while Q_n increases, resulting in atomic diffusion a dominant factor in the nucleation process. Hence, the nucleation work $\Delta G^* + Q_n$ increases with increasing pressure. Consequently, nucleation rate I decreases with the increase in pressure and an enhancement of

crystallization temperature is expected, as observed for the $Al_{89}La_6Ni_5$ amorphous alloy in the pressure range of 1–4 GPa in Fig. 9.

In addition to the aforementioned factors, the crystallization temperature(s) of an amorphous phase significantly depend on the heating rate used in DSC measurement (Kissinger, 1957). In contrast, the heating rate has a slight influence on the glass transition temperature. All these transformation temperatures of amorphous alloys increase with increasing the heating rate that is used in DSC. Therefore, the heating rate is usually indicated when describing the transformation temperatures of an amorphous phase.

4. Kinetics of crystallization

The kinetics of crystallization of amorphous alloys has been extensively studied by using differential scanning calorimetry (DSC) or differential thermal analysis (DTA), as the structural change in a material upon heating or cooling is indicated by a defection or peak in the DSC/DTA curve. The kinetic behavior associated with a structural change leading to an alternative metastable state in an amorphous alloy above its glass transition is a key subject since it provides new opportunities for structural control by innovative design and processing strategies. *Section 5* will show some application examples by controlling crystallization from amorphous precursors in order to tailor microstructure for excellent properties. Such crystallization control requires fundamental understanding of the specific mechanisms influencing structural transformations.

In general, crystallization is a thermally activated reaction, either by isothermal or isochronal heating. The transformation rate during a reaction could be described as

$$d\alpha / dt = f(\alpha)k(T) \tag{2}$$

where a is the fraction transformed. The temperature dependent function is generally assumed to follow an Arrehnius type dependency

$$k = k_0 \exp(-E / RT) \tag{3}$$

where k_0 is the reaction constant, R is the gas constant and E is the activation energy. In general, the reaction function $f(\alpha)$ is unknown. From the above equations it follows that for transformation studies by performing studies at a constant temperature T, E can be obtained as below:

$$ln\left(t_f\right) = E / RT + c_i \tag{4}$$

where t_f is the time needed to reach a certain fraction transformed, and c_i is a constant, which depends on the reaction stage and on the kinetic model. Thus, E can be obtained from two or more experiments at different T. For isothermal experiments $k(T)$ is constant, the determination of $f(\alpha)$ is relatively straightforward, and is independent of E. For non-isothermal experiments, the reaction rate at all times depends on both $f(\alpha)$ and $k(T)$, and the determination of $f(\alpha)$, k_0 and E (the so-called kinetic triplet) is an interlinked problem. A deviation in the determination of any of the three parameters will cause a deviation in the other parameters of the triplet. Over the past decades a variety of non-isothermal methods have been proposed. Among them, the Kissinger method (Kissinger, 1957) is widely used in

the isochronal method for the calculation of the activation energy for the crystallization. A higher value of the activation energy is generally interpreted as a measure of the high stability and resistance of the amorphous phase towards crystallization. The activation energy for crystallization could be determined using

$$ln\left(\beta / T_p^2\right) = -E / RT_p + C \tag{5}$$

where β is the heat rates that used to heating amorphous samples in DSC, T_p is the temperature corresponding to the peak of the crystallization event (exothermic peak), R is the gas constant and C is a constant. Thus, by plotting $ln\left(\beta / T_p^2\right)$ against $1/T_p$, one could obtain a straight line whose slope is $-E/R$, from which the activation energy for the transformation, E, can be calculated.

On the other hand, kinetic data on first-order transformations are often obtained by isothermal analysis. The isothermal crystallization kinetics of the amorphous phase can be usually analyzed in terms of the generalized theory of the well-known Kolmogorov-Johnson-Mehl-Avrami (JMA) equation (Christian, 2002) for a phase transition:

$$x_c(t,T) = 1 - \exp[-k(t-\tau)^n] \tag{6}$$

or

$$ln\left[-ln\left(1 - x_c(t,T)\right)\right] = n\,lnk + n\,ln(t-\tau) \tag{7}$$

where $x_c(t,T)$ is the volume fraction of crystallized phases after annealing time t, τ is the incubation period of transient nucleation, which is the time period that must elapse prior to formation of nuclei, k is a temperature-dependent kinetic parameter and n is the Avrami exponent, which is a significant parameter to describe the crystallization mechanism, such as nucleation and growth behavior, and varies from 1 to 4 (Doherty, 1996). For diffusion-controlled growth, one may have the following cases: $1 < n < 1.5$ indicates growth of particles with an appreciable initial volume; $n = 1.5$ indicates growth of particles with a nucleation rate close to zero; $1.5 < n < 2.5$ reflects growth of particles with decreasing nucleation rate; $n = 2.5$ reflects growth of particles with constant nucleation rate, and $n > 2.5$ pertains to the growth of small particles with an increasing nucleation rate (Doherty, 1996). A JMA plot of $\ln[-\ln(1- x_c(t,T))]$ vs. $\ln(t-\tau)$ yields a straight line with slop n and intercept $n\ln k$. Using a DSC, operated under isothermal mode, phase transformations can be distinguished unambiguously in terms of those occurring only by growth of existing nuclei or those occurring by nucleation and growth. For a transformation resulting in grain growth or structural relaxation results in a monotonically decreasing signal, a "bell-shape" exothermic curve is the classical signature for a nucleation-and growth transformation (Chen & Spaepen, 1991).

The transformed volume fraction, x, during the isothermal process at a particular temperature, T, can then be determined by measuring the area under the exothermic curve. It is assumed that the volume fraction transformed, x, up to any time, t, is proportional to the fractional area of the exothermic peak or the integrated enthalpy. Therefore, in the isothermal DSC scans, the transformed volume fraction, $x_c(t,T)$, up to any time t is

proportional to the fractional areas of the exothermic peak. Hence, the crystallized volume fraction during the isothermal annealing process can be accurately determined by measuring the area of the exothermic peak. The crystallized fractions $x_c(t,T)$ after time t at a certain temperature T for amorphous phase could be derived from the isothermal DSC curves by assuming that $x_c(t,T)$ is proportional to the integrated enthalpy

$$x_c(t,T) = \int_0^t h(t,T)\,dt \Big/ \int_0^\infty h(t,T)\,dt \tag{8}$$

where $h(t,T)$ is the enthalpy release. Using the JMA equation, the reaction rate as well as the parameters governing the nucleation rate and/or the growth morphology can be obtained. As shown before, it is inappropriate to describe the crystallization mechanism by using the average Avrami exponent derived from the non-linear JMA plot in the whole range of volume fraction. An alternative method of examining the isothermal DSC results is to evaluate the local value of the Avrami exponent, N_{loc}, which is defined as (Calka & Radlinski, 1988)

$$N_{loc} = \partial ln\left[-ln\left(1-x_c(t,T)\right)\right] / \partial \ln(t-\tau) \tag{9}$$

as a function of crystallized volume fraction $x_c(t,T)$. Such a differential Avrami plot can highlight changes in reaction kinetics during the progress of crystallization.

The isothermal activation energy for the crystallization process can also be determined in terms of the incubation period τ at different temperatures during isothermal annealing, using the Arrhenius equation for a thermally activated process (Luborsky, 1977):

$$\tau = \tau_0(-E_{iso} / RT) \tag{10}$$

where τ_0 is a constant and E_{iso} is the activation energy for crystallization. The plot of $\ln\tau$ vs. $1/T$ yields a straight line. From the slope, the activation energy E_{iso} for crystallization of an amorphous phase is calculated.

Samples	Temperature range (K)	n	$x_c(t,T)$ range	E_{iso} (kJ/mol)	E_x (kJ/mol)
$Ti_{50}Cu_{18}Ni_{22}Al_4Sn_6$	735-755	2.5-3.3	0.05-0.60	399±55	392±17
with 10 vol.% TiC	723-750	2.1-2.8	0.05-0.60[a]	384±10	382±22

[a] 0.05-0.40 was used for the composite at 723 K.

Table 2. Avrami exponent (n) and activation energy of crystallization ($E_{x\tau}$) in terms of incubation time during isothermal annealing and the activation energy of crystallization (E_{iso}) determined from a Kissinger plot for the ball-milled amorphous $Ti_{50}Cu_{18}Ni_{22}Al_4Sn_6$ alloy and its composite containing 10 vol.% TiC. Reprinted from (Zhang, et al., 2006a), with permission from American Institute of Physics.

Table 2 compares the active energy of crstallization estimated by the aforementioned two methods for the ball-milled amorphous $Ti_{50}Cu_{18}Ni_{22}Al_4Sn_6$ alloy and its composite containing 10 vol.% TiC (Zhang, et al., 2006a). As seen from Table 2, there are no essential differences in the activation energies between those evaluated using the Arrhenius equation

in isothermal annealing and those obtained by isochronal annealing as revealed by Kissinger analysis for the Ti-based amorphous alloy with and without TiC particles. The activation energy of crystallization determined from the Kissinger analysis and the Arrhenius equationfor both powders show that the composite has slightly lower activation energy. The addition of 10 vol.% TiC particles into the Ti-based amorphous alloy may slightly affect the crystallization kinetics of the amorphous phase and the TiC particles may act as potential heterogeneous nucleation sites.

5. Crystallization control for applications

5.1 Nanocrystalline alloy created from amorphous precursor via partial crystallization

The subject of preparation of nanostructured alloys by nanocrystallization of amorphous solid precursors has been reviewed by Lu (Lu, 1996) and by McHenry et al. (McHenry et al., 1999). The formation of nanocrystalline structures during crystallization of amorphous alloys is of a great interest from both the fundamental and the technical point of view. Fundamental studies of the mechanisms of crystal nucleation and growth as well as kinetics of transformation will to a certain degree aid in tailoring the structure for excellent physical (e.g. magnetic properties) and mechanical properties of nanostructured materials attractive for practical applications. In general, this method has extensively applied for those amorphous alloys where ductile solid solution phase(s) or functional phase(s) is formed through primary crystallization. Amorphous alloys of appropriate chemical compositions, crystallized at temperatures above their primary crystallization temperature but below the secondary crystallization temperature, can yield nanocrystalline grains dispersed in an amorphous matrix. Three important groups of nanocrystalline materials produced by primary crytallization from amorphous alloy precursors can be distinguished: constructional Al-based alloys (Kim et al., 1990; Latuch et al., 1997; Zhong et al., 1997), magnetically soft (Lachowicz & Slawskawaniewska, 1994; Makino et al., 1997; Suzuki et al., 1990; Suzuki et al., 1993; Willard et al., 1998) and magnetically hard (Inoue et al., 1995b; Manaf et al., 1993; Takeuchi et al., 1997; Withanawasam et al., 1994) Fe-based alloys. Examples of the alloys compositions and main aspects of their structure are presented in Table 3. There are two basic parameters characterizing structure of these materials: crystallite diameter, D, and volume fraction, V_{cr}, of nanocrystals. The optimum amount of nanocrystalline phase differs from each group. In the case of magnetically hard nanocrystalline materials, full (Manaf, et al., 1993; Takeuchi, et al., 1997) or almost full (Inoue, et al., 1995b) crystallization is required. For constructional and magnetically soft nanocrystalline materials the optimum mechanical and magnetic properties, respectively, are obtained after partial crystallization of their amorphous precursors (Inoue et al., 1988), which means that they are dual-phase materials composed of nanocrystals and an amorphous matrix. To preserve ductility in Al-based nanocrystalline alloys, V_{cr} should not exceed 20% in ternary Al–Y–Ni (Inoue, et al., 1988) and 40% in quaternary Al–Y–Ni–Cu (Latuch, et al., 1997) alloys. Mechanical properties of these materials can be explained and predicted using mixture model based on the volume fractions of amorphous matrix and nanocrystals, proposed by Kim et al. (Kim et al., 1999).

Inoue and Kimura (Inoue & Kimura, 2000) have summarized the microstructure and mechanical properties of aluminum based alloys produced by controlling the crystallization of amorphous alloy precursors, as shown in Fig. 10. A high mechanical strength exceeding

1000 MPa is achieved by the formation of an amorphous phase. The bulk nanocrystalline alloys, which contain a mixed structure of intermetallic compounds embedded fcc-Al matrix by the crystallization of Al-based amorphous phase, exhibit high mechanical strength of 700–1000 MPa and have been commercialized as a commercial name of GIGAS. By controlling the crystallization of Al-based amorphous alloys, the tensile strength of the Al-based amorphous alloys increases to 1560 MPa by the homogeneous precipitation of nanoscale fcc-Al particles into an amorphous phase, which is higher than the strength of 1260 MPa by the formation of an amorphous single phase.

Nanocrystalline materials	Magnetically soft (Fe-based)	Constructional (Al-based)	Magnetically hard (Fe-based)
Alloys	Finemet® ($Fe_{73.5}Cu_1Nb_3Si_{13.5}B_9$)	Al–RE–TM (RE=Y, Ce, Nd, Sm; TM=Ni, Co, Fe, Cu)	Fe–RE–B
	Nanoperm® ($Fe_{84}Zr_{3.5}Nb_{3.5}B_8Cu_1$)		e.g. $Fe_{82.3}Nd_{11.8}B_{5.9}$ $Fe_{88}Nb_2Pr_5B_5$
	Hitperm ($Fe_{44}Co_{44}Zr_7B_4Cu_1$)	GIGAS®	
Structure	Nanocrystals (bcc-Fe) + Amorphous matrix	Amorphous matrix + Nanocrystals (fcc-Al)	Nanocrystals $Fe_{14}Nd_2B$ (+Fe_3B, bcc-Fe, Am)
Sructural parameters			
V_{cr}	70–75% $\Rightarrow \lambda_s \approx 0$	≤ 40% $\Rightarrow$ ductility	≤ 100%
D	≤ 15 nm $\Rightarrow$ $\langle K \rangle \approx 0$	$V_{cr} \uparrow$, $D \downarrow \Rightarrow \sigma_f \uparrow$	< 25 nm
Properties	High permeability, low magnetic losses	High specific strength at high temperatures	High coercivity, high remanence

Table 3. General characteristics of the three main groups of nanocrystalline materials produced by devitrification of amorphous alloys (V_{cr} – volume fraction of crystalline phase, D – diameter of nanocrystals, λ_s – saturation magnetostriction constant, $\langle K \rangle$ – averaged magnetocrystalline anisotropy, σ_f – fracture strength). Reprinted from (Kulik, 2001), with permission from Elsevier.

5.2 Net-shape (micro-)forming in supercooled liquid region

Although amorphous alloys have exhibited unique properties compared the conventional polycrystalline materials, the metastable nature of amorphous phase has imposed a barrier to broad commercial adoption, particularly where the processing requirements of these alloys conflict with conventional metal processing methods. In general, amorphous alloys are super-strong with compressive yield strengths of approximately 2 GPa and even up to 5 GPa for some exotic bulk glass-forming alloys, as has already shown in Fig. 1. However, amorphous alloys suffer from a strong tendency toward shear localization upon yielding, which results in macroscopically brittle failure at ambient temperatures. Therefore, processing of amorphous alloys at ambient temperatures is extremely hard. When an amorphous solid is continuously heated in the supercooled liquid region the viscosity decreases dramatically as the alloy relaxes into the metastable equilibrium state of the supercooled liquid and the large viscous flowability is obtained (Bakke et al., 1995; Volkert

& Spaepen, 1989). Larger values of ΔT_x (T_x – T_g) indicate higher metastability of the liquid with respect to crystallization. The considerable softening of an amorphous alloy (viscous flowability) in its supercooled liquid region can be used for net-shape micro-forming of bulk amorphous alloy components and creation of bulk amorphous alloy samples via powder processing of amorphous powder precursors (see S*ection 5.3*). In order to maintain their unique properties, processing of an amorphous alloy requires special attention. The main challenge is to avoid crystallization during the processing of amorphous alloy. By utilizing the low viscosity and large viscous flowability, bulk amorphous alloys could be deformed (Inoue & Takeuchi, 2002; Nishiyama & Inoue, 1999) to various complicated shapes in the maintenance of good mechanical properties. For example, from a bulk amorphous $Pd_{40}Cu_{30}Ni_{10}P_{20}$ alloy rod in 6 mm diameter, the die-forging into a three-stage die with pitch circle diameters of 4, 5 and 6 mm and a module of 0.3 was made for 120 s at 610 K under a compressive stress of 10 kPa and a three-stage gear was formed. The shape and dimension

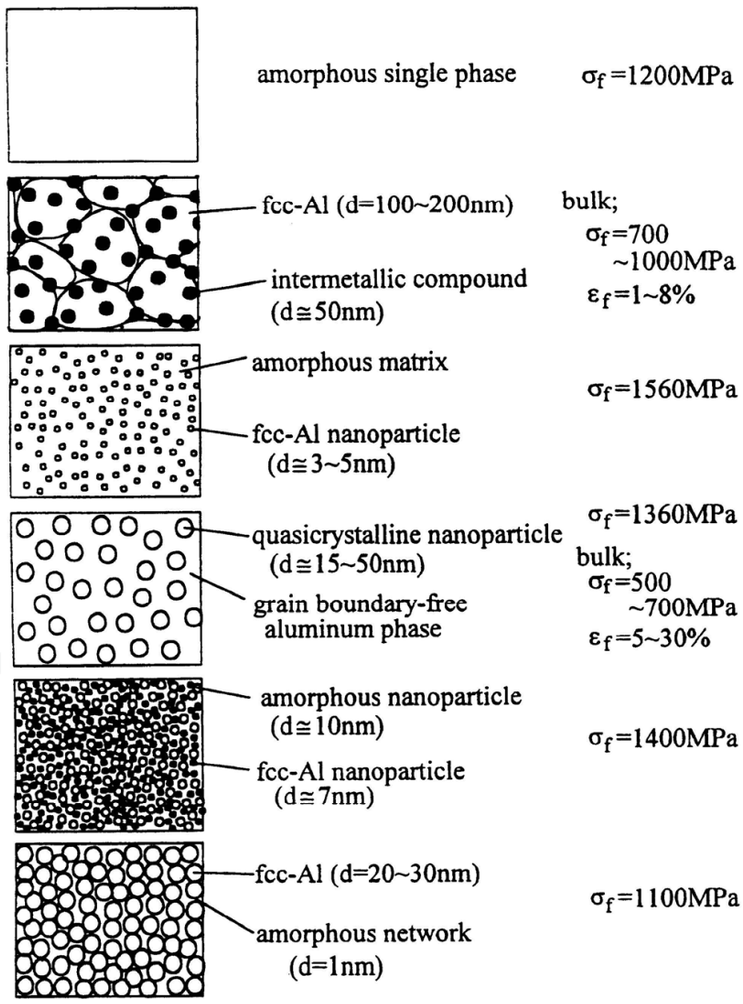

Fig. 10. Summary of the microstructure and mechanical properties of aluminum based alloys produced from amorphous alloy precursors. Reprinted from (Inoue & Kimura, 2000), with permission from Elsevier.

of the gear agree with the inner size of the die within a scattering of ±1% (Nishiyama & Inoue, 1999). The utilization of viscous flow of supercooled liquid is useful for secondary working of the bulk amorphous alloys which can produce a final product with near-net shape. In addition, in the supercooled liquid region, successful joining of the $Pd_{40}Ni_{40}P_{20}$ bulk amorphous components has been achieved by the friction-welding method utilizing the viscous flowability of the supercooled liquid (Kawamura & Ohno, 2001).

Recently, Schroers and his co-workers (Kumar et al., 2009; Schroers et al., 2007; Schroers, 2008; 2010; Schroers et al., 2011) have used a developed novel thermoplastic forming (TPF)-based processing to fabricate complex amorphous components. The process of TPF is also known as hot forming, hot pressing, super plastic forming, viscous flow working, and viscous flow forming. TPF takes advantage of the drastic softening of amorphous alloys upon heating above glass transition temperature and its thermal stability of supercooled liquid, which is quantified by the width of the supercooled liquid region. During TPF, the amorphous

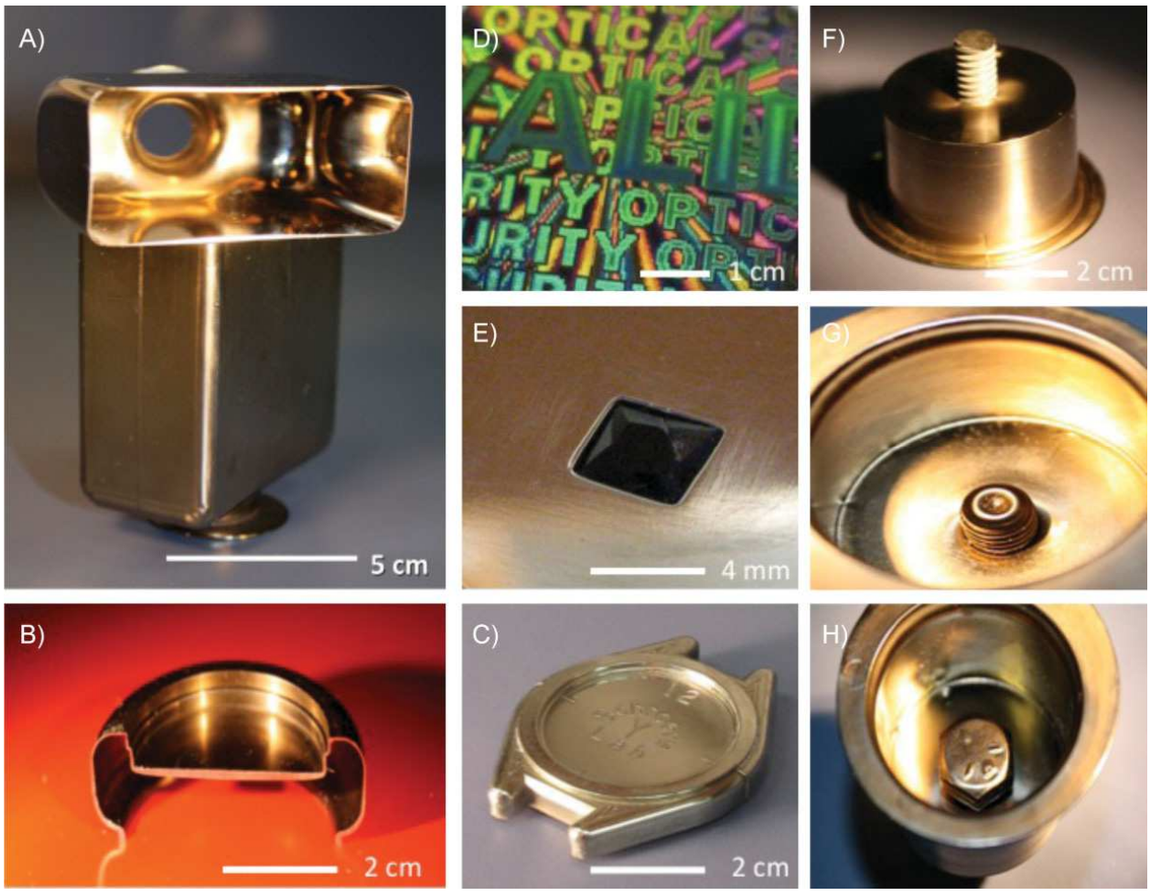

Fig. 11. Through TPF-based blow molding Blow molding with bulk metallic glasses (BMGs) permits hollow, thin, seamless shapes, which can include undercuts. These shapes were previously unachievable with any other metal processing method (A–C). The surface can be patterned, e.g., to reveal a hologram (D), joints can be created such as threads (F,H), and a second material can be joined to the BMG (E) in the same processing step than the blow molding. Reprinted from (Schroers, 2010), with permission from John Wiley and Sons.

solid is reheated into the supercooled liquid region, where it relaxes into a supercooled and metastable liquid before it eventually crystallizes. For a variety of BMG formers, a large processing window exists, which permits access to temperatures in this region on a practical experimental time scale in order to avoid crystallization. In general, at low temperatures a long processing time is available accompanied by a high viscosity. In contrast, at high temperatures, the viscosity is significantly reduced but, at the same time, the processing time is shortened. Currently, for a wide range of alloys, viscosities of 10^6 Pa s and lower can be accessed in the supercooled liquid region on a practical time scale (Schroers, 2010). For the highest formability of the BMG former in supercooled liquid region, optimum processing such as low viscosity and long processing time are required. The formability is a material property that reflects the maximum strain a metastable material can undergo before crystallization under given geometry and processing parameters.

As a novel technique with integration of shaping, joining, and finishing into one processing step, TPF-based blow molding allows one to net shape complex geometries in an economical and precise manner, including shapes, which can not be produced with any other metal processing method. In particular when pre-shaped parisons are used, BMGs can be blow molded into shapes that were previously not achievable with any metal processing method. Examples of such shapes are given in Fig. 11. They include hollow seamless shapes, which can comprise of complex undercuts, and very large thin sections. Due to the low forming pressure, together with the ability to replicate smallest features, as shown in Fig. 11D, the dimensional accuracy that can be achieved with this process is even superior over other TPF-based processes. In addition, this method is capable to combine the three processing steps typically required for metal processing—shaping, joining, and finishing—into one step (Schroers, 2010). For example potential joints such as threads, as shown in Fig. 11E–H can be formed in the BMG during the expansion process. Surface finishes that can be achieved with blow molding of BMGs include mirror finish. The superior properties of BMGs relative to plastics and typical structural metals, combined with the ease, economy, and precision of blow molding, have the potential to impact society in a manner similar to the development of synthetic plastics and their associated processing methods.

5.3 Bulk amorphous alloy consolidated from amorphous powder precursor

Synthesis of three-dimensional bulk amorphous materials has been an attractive object for several decades, not only for its significance in basic studies of the intrinsic properties of bulk amorphous materials (instead of the form of powders, fibers, or ribbons), but also for technological applications of these advanced materials with many novel properties. In principle, there are two approaches to obtain bulk amorphous samples. The first one is direct casting of alloy melts into bulk form in amorphous state (Suryanarayana & Inoue, 2011). An alternative approach that can potentially lead to bulk amorphous alloys is to exploit the viscous flow resulting from the significant decrease of the viscosity in supercooled liquid region. This is an especially attractive route to bulk amorphous alloys, especially to obtain bulk samples for the alloy systems with insufficient or limited glass-forming ability. A number of amorphous alloys with a sizable supercooled liquid region have been reported (Inoue, 2000; Johnson, 1999). This opens up the possibility of preparing truly bulk samples through powder consolidation in supercooled liquid region. In the Zr-, Cu-, Fe- and Ni-based alloy systems, some successful consolidation of amorphous powders

with wide supercooled liquid region has been achieved by warm extrusion, spark plasma sintering and equal channel angular pressing (ECAP) (Choi et al., 2007; Ishihará et al., 2002; Itoi et al., 2001; Karaman et al., 2004; Kawamura et al., 1997; Kim et al., 2004; Kim et al., 2009; Lee et al., 2003; Mear et al., 2009; Robertson et al., 2003; Senkov et al., 2004; Senkov et al., 2005; Sordelet et al., 2002; Zhang et al., 2006b; Zhang, et al., 2007a). The consolidated samples show almost the same thermal properties, mechanical properties, and/or soft magnetic properties as those of the BMGs prepared by direct melt casting from molted

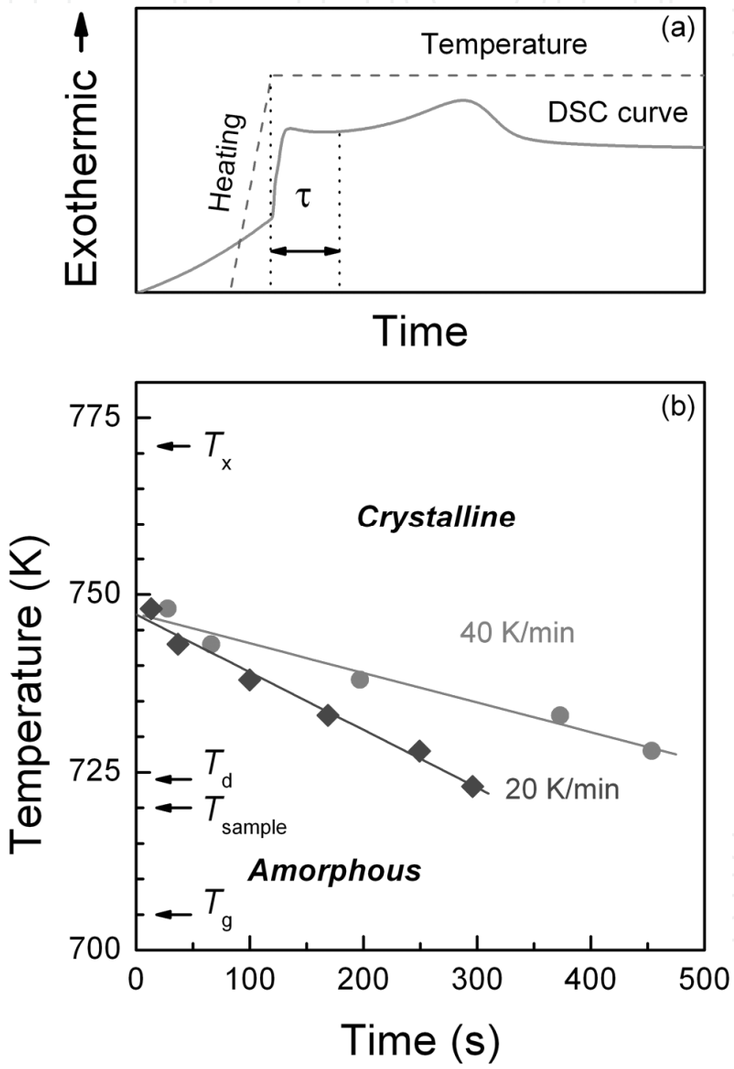

Fig. 12. (a) A representative DSC curve to determine the holding time (τ) up to the initial crystallization, and (b) TTT diagram for the onset of crystallization of the amorphous $Ti_{50}Cu_{18}Ni_{22}Al_4Sn_6$ powders heated to set temperatures at heating rate of 0.33 or 0.67 K s^{-1}. The data of the onset temperature of crystallization (T_x) and the glass transition temperature (T_g) at the heating rate of 0.67 K s^{-1} are also shown. Reprinted from (Zhang, et al., 2006b), with permission from Elsevier.

liquid. Among the aforementioned consolidation methods, it has recently been shown that ECAP is a particular effective and novel approach used for the consolidation of amorphous powders. ECAP is a method for subjecting a volume fraction of materials to severe shear deformation by forcing them around a mold corner (Karaman, et al., 2004; Robertson, et al., 2003; Zhang, et al., 2006b). The advantages of ECAP have allowed to fabricate bulk materials with large cross-sections.

In order to utilize the viscous flow of amorphous phase, the crystallization of an amorphous alloys must be well controlled. Therefore, the temperature–time–transformation (TTT) diagram should be determined for the selected amorphous powders by measuring the onset time of the exothermic reaction due to crystallization on the DSC curves during isothermal annealing (e.g. see Fig. 12 (a)), where the sample was heated to the selected annealing temperature(s) in the supercooled liquid region, and the time that the sample began to crystallize (the onset of an exothermic reaction) was recorded. Fig. 12 (b) shows an example of the TTT diagram for the amorphous $Ti_{50}Cu_{18}Ni_{22}Al_4Sn_6$ powders, which provides a window for processing in supercooled liquid state. The temperature and the time before crystallization (or the time to remain in the fully amorphous state at a certain temperature) exhibits approximately a linear relationship. At a given heating rate, the lower the temperature is, the longer the time is for the supercooled liquid to remain stable without crystallization. For the same temperature, the time window is longer at a faster heating rate. Therefore, for the ECAP processing at a given length of the can, it is necessary to select a suitable extrusion temperature (T_e) and extrusion rate (v_e). Two extrusion temperatures (700 and 705 K) near the calorimetric glass transition temperature (T_g) were used in when with extrusion rate of 0.40 mm s^{-1} (Zhang, et al., 2006b). By using ECAP with these processing parameters, bulk nanocrystal-amorphous composites with a relative density about 97% have been achieved from the amorphous $Ti_{50}Cu_{18}Ni_{22}Al_4Sn_6$ powders. Full densification was not reached, mainly owing to that the powders experienced insufficient shear deformation and that partial crystallization occurred during ECAP processing (Zhang, et al., 2006b).

Karaman et al (Karaman, et al., 2004) has optimized the ECAP process to consolidate the gas-atomized Vitreloy 106a ($Zr_{58.5}Nb_{2.8}Cu15.6Ni_{12.8}Al_{10.3}$) powder in supercooled liquid region at different strain rates and temperatures. The microstructure of all consolidates shows significant particle deformation. The increase in aspect ratio of particles due to shear strain is correlated with the extrusion temperature. Extrusions processed close to glass transition temepraure showed significant porosity. There is an increase in the consolidate hardness, depending on the extrusion temperature. Compression experiments on the consolidated V106a shows that good consolidate samples have strength levels of 1500 – 1700 MPa, which are comparable to that of cast V106 ($Zr_{57}Nb_5Al_{10}Cu_{15.4}Ni_{12.6}$). In spite of some nanocrystallization and short-range order formation upon processing, most of the fracture surfaces of the consolidates show shear banding and well-developed vein patterns, typical fracture characteristics of amorphous alloys with good ductility.

6. Conclusions

The amorphous alloys have attracted widespread research interests because of their technological promise for practical applications due to execellent properties and scientific

importance in understanding glass formation and glass phenomena. Due to the nature of metastability, amorphous phase tends to crystalize to more stable crystalline state through *polymorphous*, *eutectic* and/or *primary* crystallization mechanisms. The crystallization mechanisms and crystallization products are influenced by both inherent (e.g. chemical composition of amorphous phase, oxygen) and extraneous (e.g. preparation method, pressure, etc.) factors. The study of kinetic behavior associated with a structural change in amorphous alloys above glass transition temperature could provide opportunities for structure control by innovative design and processing strategies. By controlling the crystallization of amorphous alloys, bulk nanocrystalline alloys and/or nanocrystalline-amorphous composites with excellent properties could be achieved from amorphous alloys precursors. By utilizing the viscous flowability of amorphous alloys in supercooled liquid region, net-shaped microforming could be realized for bulk amorphous alloys and bulk amorphous components with "true" bulk size might be produced from amorphous powder precursors.

7. Acknowledgments

The author is grateful to J. Xu, E. Ma, J. Eckert, H.B. Lu and M. Calin for their stimulating discussions. Financial support provided by Research Services of The University of Western Australia (through UWA Research Development Award Scheme) is gratefully acknowledged.

8. References

Altounian, Z.; Batalla, E.; Stromolsen, J.O. & Walter, J.L. (1987). The influence of oxygen and other impurities on the crystallization of NiZr2 and related metallic glasses. *Journal of Applied Physics,* Vol. 61, No. 1, (January 1987), pp. 149-155, ISSN 0021-8979

Azam, N.; Lenaour, L.; Rivera, C.; Grosjean, P.; Sacovy, P. & Delaplace, J. (1979). Crystallization and irradiation effects of amorphous Fe40Ni38Mo4B18 alloy. *Journal of Nuclear Materials,* Vol. 83, No. 2, (Febuary 1979), pp. 298-304, ISSN 0022-3115

Bakke, E.; Busch, R. & Johnson, W.L. (1995). The viscosity of the Zr46.75Ti8.25Cu7.5Ni10Be27.5 bulk metallic-glass forming alloy in the supercooled liquid. *Applied Physics Letters,* Vol. 67, No. 22, (November 1995), pp. 3260-3262, ISSN 0003-6951

Calin, M.; Zhang, L.C. & Eckert, J. (2007). Tailoring of microstructure and mechanical properties of a Ti-based bulk metallic glass-forming alloy. *Scripta Materialia,* Vol. 57, No. 12, (December 2007), pp. 1101-1104, ISSN 1359-6462

Calka, A. & Radlinski, A.P. (1988). The local value of the avrami exponent - a new approach to devitrification of glassy metallic ribbons. *Materials Science and Engineering,* Vol. 97, No. 1, (January 1988), pp. 241-246, ISSN 0025-5416

Chen, H.S. & Turnbull, D. (1969). Formation, stability and structure of Palladium-Silicon based alloy glasses. *Acta Metallurgica,* Vol. 17, No. 8, (August 1969), pp. 1021-1031, ISSN 0001-6160

Chen, L.C. & Spaepen, F. (1991). Analysis of calorimetric measurements of grain-growth. *Journal of Applied Physics,* Vol. 69, No. 2, (January 1991), pp. 679-688, ISSN 0021-8979

Choi, P.P.; Kim, J.S.; Nguyen, O.T.H.; Kwon, D.H.; Kwon, Y.S. & Kim, J.C. (2007). A1-La-Ni-Fe bulk metallic glasses produced by mechanical alloying and spark-plasma

sintering. *Materials Science and Engineering A,* Vol. 449, No. 1-2, (March 2007), pp. 1119-1122, ISSN 0921-5093

Christian, J.W. (2002). *The Theory of Transformations in Metals and Alloys* (3rd ed.). Elsevier Science, ISBN 9780080440194, Oxford

Doherty, R.D. (1996). Diffusive phase transformations In the solid state. In: Cahn, R.W. & Haasen, P. (Eds.), *Physical metallurgy* (Fourth, revised and enhanced edition ed., Vol. II, pp. 1363-1506). Amsterdam: North-Hollaiw.

Dong, Z.F.; Ma, Y.H. & Lu, K. (1994). Crystallization process and thermal stabilities of the melt-spun amorphous Ni100-xPx (x=16.0-20.0 at-percent) alloys. *Scripta Metallurgica et Materialia,* Vol. 31, No. 1, (July 1994), pp. 81-86, ISSN 0956-716X

Eckert, J.; Mattern, N.; Zinkevitch, M. & Seidel, M. (1998). Crystallization behavior and phase formation in Zr-Al-Cu-Ni metallic glass containing oxygen. *Materials Transactions JIM,* Vol. 39, No. 6, (June 1998), pp. 623-632, ISSN 0916-1821

Eckert, J.; Kuhn, U.; Mattern, N.; Reger-Leonhard, A. & Heilmaier, M. (2001). Bulk nanostructured Zr-based multiphase alloys with high strength and good ductility. *Scripta Materialia,* Vol. 44, No. 8-9, (May 2001), pp. 1587-1590, ISSN 1359-6462

Eckert, J.; Das, J.; Pauly, S. & Duhamel, C. (2007). Mechanical properties of bulk metallic glasses and composites. *Journal of Materials Research,* Vol. 22, No. 2, (Febuary 2007), pp. 285-301, ISSN 0884-2914

Foley, J.C.; Allen, D.R. & Perepezko, J.H. (1997). Strategies for the development of nanocrystalline materials through devitrification. *Materials Science and Engineering A,* Vol. 226, No. 1-2, (June 1997), pp. 569-573, ISSN 0921-5093

Fornell, J.; Rossinyol, E.; Surinach, S.; Baro, M.D.; Li, W.H. & Sort, J. (2010). Enhanced mechanical properties in a Zr-based metallic glass caused by deformation-induced nanocrystallization. *Scripta Materialia,* Vol. 62, No. 1, (January 2010), pp. 13-16, ISSN 1359-6462

Gebert, A.; Eckert, J. & Schultz, L. (1998). Effect of oxygen on phase formation and thermal stability of slowly cooled Zr65Al7.5Cu7.5Ni10 metallic glass. *Acta Materialia,* Vol. 46, No. 15, (September 1998), pp. 5475-5482, ISSN 1359-6454

He, Y.; Schwarz, R.B. & Archuleta, J.I. (1996). Bulk glass formation in the Pd-Ni-P system. *Applied Physics Letters,* Vol. 69, No. 13, (September 1996), pp. 1861-1863, ISSN 0003-6951

Hono, K.; Hiraga, K.; Wang, Q.; Inoue, A. & Sakurai, T. (1992). The microstructure evolution of a Fe73.5Si13.5B9Nb3Cu1 nanocrystalline soft magnetic material. *Acta Metallurgica Et Materialia,* Vol. 40, No. 9, (September 1992), pp. 2137-2147, ISSN 0956-7151

Illeková, E.; Jergel, M.; Duhaj, P. & Inoue, A. (1997). The relation between the bulk and ribbon Zr55Ni25Al20 metallic glasses. *Materials Science and Engineering A,* Vol. 226-228, No. 1-2, (June 1997), pp. 388-392, ISSN 0921-5093

Inoue, A.; Ohtera, K.; Tsai, A.P. & Masumoto, T. (1988). New amorphous-alloys with good ductility in Al-Y-M and Al-La-M (M=Fe, Co, Ni or Cu) systems. *Japanese Journal of Applied Physics,* Vol. 27, No. 3, (March 1988), pp. L280-L282, ISSN 0021-4922

Inoue, A.; Kita, K.; Zhang, T. & Masumoto, T. (1989). An Amorphous La55Al25Ni20 Alloy Prepared by Water Quenching. *Materials Transactions JIM,* Vol. 30, No. 9, (September 1989), pp. 722-725, ISSN 0916-1821

Inoue, A.; Nakamura, N.; Sugita, T.; Zhang, T. & Masumoto, T. (1993a). Bulky La–Al–TM (TM=Transition Metal) amorphous alloys with high tensile strength produced by a

high-pressure die casting method. *Materials Transactions JIM,* Vol. 34, No. 4, (April 1993), pp. 351-358, ISSN 0916-1821

Inoue, A.; Zhang, T.; Nishiyama, N.; Ohba, K. & Masumoto, T. (1993b). Preparation of 16 mm diameter rod of amorphous Zr65Al7.5Ni10Cu17.5 alloy. *Materials Transactions JIM,* Vol. 34, No. 12, (December 1993), pp. 1234-1237, ISSN 0916-1821

Inoue, A.; Shinohara, Y.; Yokoyama, Y. & Masumoto, T. (1995a). Solidification analyses of bulky Zr60Al10Ni10Cu15Pd5 glass produced by casting into wedge-shape copper mold. *Materials Transactions JIM,* Vol. 36, No. 10, (October 1995), pp. 1276-1281, ISSN 0916-1821

Inoue, A.; Takeuchi, A.; Makino, A. & Masumoto, T. (1995b). Hard magnetic-properties of nanocrystalline Fe-rich Fe-Nd-B alloys prepared by partial crystallization of amorphous phase. *Materials Transactions JIM,* Vol. 36, No. 7, (July 1995), pp. 962-971, ISSN 0916-1821

Inoue, A.; Nishiyama, N. & Kimura, H. (1997). Preparation and Thermal Stability of Bulk Amorphous Pd40Cu30Ni10P20 Alloy Cylinder of 72 mm in Diameter. *Materials Transactions JIM,* Vol. 38, No. 2, (February 1997), pp. 179-183, ISSN 0916-1821

Inoue, A. (2000). Stabilization of metallic supercooled liquid and bulk amorphous alloys. *Acta Materialia,* Vol. 48, No. 1, (January 2000), pp. 279-306, ISSN 1359-6454

Inoue, A. & Kimura, H. (2000). High-strength aluminum alloys containing nanoquasicrystalline particles. *Materials Science and Engineering A,* Vol. 286, No. 1, (June 2000), pp. 1-10, ISSN 0921-5093

Inoue, A. & Takeuchi, A. (2002). Recent progress in bulk glassy alloys. *Materials Transactions,* Vol. 43, No. 8, (August 2002), pp. 1892-1906, ISSN 1345-9678

Inoue, A.; Shen, B.L. & Chang, C.T. (2004a). Super-high strength of over 4000 MPa for Fe-based bulk glassy alloys in [(Fe1−xCox)0.75B0.2Si0.05]96Nb4 system. *Acta Materialia,* Vol. 52, No. 14, (August 2004), pp. 4093-4099, ISSN 1359-6454

Inoue, A.; Shen, B.L.; Koshiba, H.; Kato, H. & Yavari, A.R. (2004b). Ultra-high strength above 5000 MPa and soft magnetic properties of Co-Fe-Ta-B bulk glassy alloys. *Acta Materialia,* Vol. 52, No. 6, (April 2004), pp. 1631-1637, ISSN 1359-6454

Inoue, A.; Zhang, W.; Tsurui, T.; Yavari, A.R. & Greer, A.L. (2005). Unusual room-temperature compressive plasticity in nanocrystal-toughened bulk copper-zirconium glass. *Philosophical Magazine Letters,* Vol. 85, No. 5, (May 2005), pp. 221-229, ISSN 0950-0839

Ishihará, S.; Zhang, W. & Inoue, A. (2002). Hot pressing of Fe-Co-Nd-Dy-B glassy powders in supercooled liquid state and hard magnetic properties of the consolidated alloys. *Scripta Materialia,* Vol. 47, No. 4, (August 2002), pp. 231-235, ISSN 1359-6462

Itoi, T.; Takamizawa, T.; Kawamura, Y. & Inoue, A. (2001). Fabrication of Co40Fe22Nb8B30 bulk metallic glasses by consolidation of gas-atomized powders and their soft-magnetic properties. *Scripta Materialia,* Vol. 45, No. 10, (November 2001), pp. 1131-1137, ISSN 1359-6462

Jiang, J.Z.; Olsen, J.S.; Gerward, L.; Abdali, S.; Eckert, J.; Schlorke-de Boer, N.; Schultz, L.; Truckenbrodt, J. & Shi, P.X. (2000). Pressure effect on crystallization of metallic glass Fe72P11C6Al5B4Ga2 alloy with wide supercooled liquid region. *Journal of Applied Physics,* Vol. 87, No. 5, (March 2000), pp. 2664-2666, ISSN 0021-8979

Jiang, J.Z.; Gerward, L. & Xu, Y.S. (2002). Pressure effect on crystallization kinetics in Zr46.8Ti8.2Cu7.5Ni10Be27.5 bulk glass. *Applied Physics Letters,* Vol. 81, No. 23, (December 2002), pp. 4347-4349, ISSN 0003-6951

Jiang, J.Z.; Saida, J.; Kato, H.; Ohsuna, T. & Inoue, A. (2003a). Is Cu60Ti10Zr30 a bulk glass-forming alloy? *Applied Physics Letters,* Vol. 82, No. 23, (June 2003), pp. 4041-4043, ISSN 0003-6951

Jiang, J.Z.; Yang, B.; Saksl, K.; Franz, H. & Pryds, N. (2003b). Crystallization of Cu60Ti20Zr20 metallic glass with and without pressure. *Journal of Materials Research,* Vol. 18, No. 4, (April 2003), pp. 895-898, ISSN 0884-2914

Jiang, X.Y.; Zhong, Z.C. & Greer, A.L. (1997). Primary crystallization in an amorphous Al88Ni4Y8 alloy. *Philosophical Magazine B,* Vol. 76, No. 4, (October 1997), pp. 419-423, ISSN 0141-8637

Johnson, W.L. (1999). Bulk glass-forming metallic alloys: Science and technology. *MRS Bulletin,* Vol. 24, No. 10, (October 1999), pp. 42-56, ISSN 0883-7694

Kang, H.G.; Park, E.S.; Kim, W.T.; Kim, D.H. & Cho, H.K. (2000). Fabrication of bulk Mg-Cu-Ag-Y glassy alloy by squeeze casting. *Materials Transactions Jim,* Vol. 41, No. 7, (July 2000), pp. 846-849, ISSN 0916-1821

Karaman, I.; Robertson, J.; Im, J.T.; Mathaudhu, S.N.; Luo, Z.P. & Hartwig, K.T. (2004). The effect of temperature and extrusion speed on the consolidation of zirconium-based metallic glass powder using equal-channel angular extrusion. *Metallurgical and Materials Transactions A,* Vol. 35A, No. 1, (January 2004), pp. 247-256, ISSN 1073-5623

Kawamura, Y.; Kato, H.; Inoue, A. & Masumoto, T. (1997). Fabrication of bulk amorphous alloys by powder consolidation. *International Journal of Powder Metallurgy,* Vol. 33, No. 2, (March 1997), pp. 50-61, ISSN 0888-7462

Kawamura, Y. & Ohno, Y. (2001). Superplastic bonding of bulk metallic glasses using friction. *Scripta Materialia,* Vol. 45, No. 3, pp. 279-285, ISSN 1359-6462

Kelton, K.F.; Croat, T.K.; Gangopadhyay, A.K.; Xing, L.Q.; Greer, A.L.; Weyland, M.; Li, X. & Rajan, K. (2003). Mechanisms for nanocrystal formations in metallic glasses. *Journal of Non-Crystalline Solids,* Vol. 317, No. 1-2, (March 2003), pp. 71-77, ISSN 0022-3093

Kim, H.J.; Lee, J.K.; Shin, S.Y.; Jeong, H.G.; Kim, D.H. & Bae, J.C. (2004). Cu-based bulk amorphous alloys prepared by consolidation of amorphous powders in the supercooled liquid region. *Intermetallics,* Vol. 12, No. 10-11, (October-November 2004), pp. 1109-1113, ISSN 0966-9795

Kim, H.S.; Warren, P.J.; Cantor, B. & Lee, H.R. (1999). Mechanical properties of partially crystallized aluminum based amorphous alloys. *Nanostructured Materials,* Vol. 11, No. 2, (March 1999), pp. 241-247, ISSN 0965-9773

Kim, J.S.; Povstugar, I.V.; Choi, P.P.; Yelsukov, E.P. & Kwon, Y.S. (2009). Synthesis of Al-Y-Ni-Co composites by mechanical alloying and consecutive spark-plasma sintering. *Journal of Alloys and Compounds,* Vol. 486, No. 1-2, (November 2009), pp. 511-514, ISSN 0925-8388

Kim, Y.H.; Inoue, A. & Masumoto, T. (1990). Ultrahigh tensile strengths of Al88Y2Ni9Mn1 or Al88Y2Ni9Fe1 amorphous-alloys containing finely dispersed fcc-Al particles. *Materials Transactions JIM,* Vol. 31, No. 8, (August 1990), pp. 747-749, ISSN 0916-1821

Kissinger, H.E. (1957). Reaction kinetics in differential thermal analysis. *Analytical Chemistry,* Vol. 29, No. 11, (November 1957), pp. 1702-1706, ISSN 0003-2700

Klement, W.; Willens, R.H. & Duwez, P. (1960). Non-crystalline structure in solidified Gold-Silicon alloys. *Nature,* Vol. 187, No. 4740, (September 1960), pp. 869-870, ISSN 0028-0836

Köster, U. & Herold, U. (1981). Crystallization of metallic glasses. In: Guntherodt, H.-J. & Beck, H. (Eds.), *Glassy Metals I, Ionic Structure, Electronic Transport, and Crystallization* (pp. 225-259). Berlin: Springer-Verlag.

Köster, U. & Meinhardt, J. (1994). Crystallization of highly undercooled metallic melts and metallic glasses around the glass-transition temperature. *Materials Science and Engineering A,* Vol. 178, No. 1-2, (April 1994), pp. 271-278, ISSN 0921-5093

Köster, U.; Meinhardt, J.; Roos, S. & Liebertz, H. (1996). Formation of quasicrystals in bulk glass forming Zr-Cu-Ni-Al alloys. *Applied Physics Letters,* Vol. 69, No. 2, (July 1996), pp. 179-181, ISSN 0003-6951

Köster, U.; Meinhardt, J.; Roos, S. & Busch, R. (1997). Formation of quasicrystals in bulk glass forming Zr-Cu-Ni-Al alloys. *Materials Science and Engineering A,* Vol. 226, No. 1-2, (June 1997), pp. 995-998, ISSN 0921-5093

Kubler, A.; Eckert, J.; Gebert, A. & Schultz, L. (1998). Influence of oxygen on the viscosity of Zr-Al-Cu-Ni metallic glasses in the undercooled liquid region. *Journal of Applied Physics,* Vol. 83, No. 6, (March 1998), pp. 3438-3440, ISSN 0021-8979

Kulik, T. (2001). Nanocrystallization of metallic glasses. *Journal of Non-Crystalline Solids,* Vol. 287, No. 1-3, (July 2001), pp. 145-161, ISSN 0022-3093

Kumar, G.; Tang, H.X. & Schroers, J. (2009). Nanomoulding with amorphous metals. *Nature,* Vol. 457, No. 7231, (Febuary 2009), pp. 868-872, ISSN 0028-0836

Lachowicz, H.K. & Slawskawaniewska, A. (1994). Coexistence of various magnetic phases in nanocrystalline Fe-based metallic glasses. *Journal of Magnetism and Magnetic Materials,* Vol. 133, No. 1-3, (May 1994), pp. 238-242, ISSN 0304-8853

Latuch, J.; Kokoszkiewicz, A. & Matyja, H. (1997). The effect of Cu addition on the formation of fcc-Al phase in rapidly quenched Al-Y-Ni alloys. *Materials Science and Engineering A,* Vol. 226-228, No. 1-2, (June 1997), pp. 809-812, ISSN 0921-5093

Lee, M.H.; Bae, D.H.; Kim, W.T.; Kim, D.H.; Rozhkova, E.; Wheelock, P.B. & Sordelet, D.J. (2003). Synthesis of Ni-based bulk amorphous alloys by warm extrusion of amorphous powders. *Journal of Non-Crystalline Solids,* Vol. 315, No. 1-2, (January 2003), pp. 89-96, ISSN 0022-3093

Lin, X.H.; Johnson, W.L. & Rhim, W.K. (1997). Effect of oxygen impurity on crystallization of an undercooled bulk glass forming Zr-Ti-Cu-Ni-Al alloy. *Materials Transactions JIM,* Vol. 38, No. 5, (May 1997), pp. 473-477, ISSN 0916-1821

Lohwongwatana, B.; Schroers, J. & Johnson, W.L. (2006). Strain rate induced crystallization in bulk metallic glass-forming liquid. *Physical Review Letters,* Vol. 96, No. 7, (Febuary 2006), pp. 075503, ISSN 0031-9007

Lu, K. (1996). Nanocrystalline metals crystallized from amorphous solids: Nanocrystallization, structure, and properties. *Materials Science and Engineering R,* Vol. 16, No. 4, (April 1996), pp. 161-221, ISSN 0927-796X

Lu, K.; Liu, X.D. & Yuan, F.H. (1996). Synthesis of the NiZr2 intermetallic compound nanophase materials. *Physica B,* Vol. 217, No. 1-2, (January 1996), pp. 153-159, ISSN 0921-4526

Luborsky, F.E. (1977). Crystallization of some Fe-Ni metallic glasses. *Materials Science and Engineering,* Vol. 28, No. 1, (April 1977), pp. 139-144, ISSN 0025-5416

Makino, A.; Bitoh, T.; Inoue, A. & Masumoto, T. (1997). Nanocrystalline Fe-M-B-Cu (M=Zr,Nb) alloys with improved soft magnetic properties. *Journal of Applied Physics,* Vol. 81, No. 6, (March 1997), pp. 2736-2739, ISSN 0021-8979

Manaf, A.; Buckley, R.A. & Davies, H.A. (1993). New nanocrystalline high-remanence Nd-Fe-B alloys by rapid solidification. *Journal of Magnetism and Magnetic Materials,* Vol. 128, No. 3, (December 1993), pp. 302-306, ISSN 0304-8853

McHenry, M.E.; Willard, M.A. & Laughlin, D.E. (1999). Amorphous and nanocrystalline materials for applications as soft magnets. *Progress in Materials Science,* Vol. 44, No. 4, (October 1999), pp. 291-433, ISSN 0079-6425

Mear, F.O.; Xie, G.Q.; Louzguine-Luzgin, D.V. & Inoue, A. (2009). Spark plasma sintering of Mg-based amorphous ball-milled powders. *Materials Transactions,* Vol. 50, No. 3, (March 2009), pp. 588-591, ISSN 1345-9678

Murty, B.S.; Ping, D.H.; Hono, K. & Inoue, A. (2000). Influence of oxygen on the crystallization behavior of Zr65Cu27.5Al7.5 and Zr66.7Cu33.3 metallic glasses. *Acta Materialia,* Vol. 48, No. 15, (September 2000), pp. 3985-3996, ISSN 1359-6454

Nicolaus, M.M.; Sinning, H.R. & Haessner, F. (1992). Crystallization behavior and generation of a nanocrystalline state from amorphous Co33Zr67. *Materials Science and Engineering A,* Vol. 150, No. 1, (Febuary 1992), pp. 101-112, ISSN 0921-5093

Nishiyama, N. & Inoue, A. (1999). Glass transition behavior and viscous flow working of Pd40Cu30Ni10P20 amorphous alloy. *Materials Transactions JIM,* Vol. 40, No. 1, (January 1999), pp. 64-71, ISSN 0916-1821

Peker, A. & Johnson, W.L. (1993). A hghly processable metallic glass: Zr41.2Ti13.8Cu12.5-Ni10.0Be22.5. *Applied Physics Letters,* Vol. 63, No. 17, (October 1993), pp. 2342-2344, ISSN 0003-6951

Robertson, J.; Im, J.T.; Karaman, I.; Hartwig, K.T. & Anderson, I.E. (2003). Consolidation of amorphous copper based powder by equal channel angular extrusion. *Journal of Non-Crystalline Solids,* Vol. 317, No. 1-2, (March 2003), pp. 144-151, ISSN 0022-3093

Sahu, K.K.; Mauro, N.A.; Longstreth-Spoor, L.; Saha, D.; Nussinov, Z.; Miller, M.K. & Kelton, K.F. (2010). Phase separation mediated devitrification of Al88Y7Fe5 glasses. *Acta Materialia,* Vol. 58, No. 12, (July 2010), pp. 4199-4206, ISSN 1359-6454

Schroers, J.; Nguyen, T.; O'Keeffe, S. & Desai, A. (2007). Thermoplastic forming of bulk metallic glass - applications for MEMS and microstructure fabrication. *Materials Science and Engineering A,* Vol. 449, No. 1-2, (March 2007), pp. 898-902, ISSN 0921-5093

Schroers, J. (2008). On the formability of bulk metallic glass in its supercooled liquid state. *Acta Materialia,* Vol. 56, No. 3, (Febuary 2008), pp. 471-478, ISSN 1359-6454

Schroers, J. (2010). Processing of Bulk Metallic Glass. *Advanced Materials,* Vol. 22, No. 14, (April 2010), pp. 1566-1597, ISSN 0935-9648

Schroers, J.; Hodges, T.M.; Kumar, G.; Raman, H.; Barnes, A.J.; Quoc, P. & Waniuk, T.A. (2011). Thermoplastic blow molding of metals. *Materials Today,* Vol. 14, No. 1-2, (January-Febuary 2011), pp. 14-19, ISSN 1369-7021

Senkov, O.N.; Miracle, D.B.; Scott, J.M. & Senkova, S.V. (2004). Equal channel angular extrusion compaction of semi-amorphous Al85Ni10Y2.5La2.5 alloy powder. *Journal of Alloys and Compounds,* Vol. 365, No. 1-2, (Febuary 2004), pp. 126-133, ISSN 0925-8388

Senkov, O.N.; Senkova, S.V.; Scott, J.M. & Miracle, D.B. (2005). Compaction of amorphous aluminum alloy powder by direct extrusion and equal channel angular extrusion. *Materials Science and Engineering A,* Vol. 393, No. 1-2, (Febuary 2005), pp. 12-21, ISSN 0921-5093

Setyawan, A.D.; Saida, J.; Kato, H.; Matsushita, M. & Inoue, A. (2010). Deformation-induced structural transformation leading to compressive plasticity in Zr65Al7.5Ni10Cu12.5M5 (M = Nb, Pd) glassy alloys. *Journal of Materials Research,* Vol. 25, No. 6, (June 2010), pp. 1149-1158, ISSN 0884-2914

Sordelet, D.J.; Rozhkova, E.; Huang, P.; Wheelock, P.B.; Besser, M.F.; Kramer, M.J.; Calvo-Dahlborg, M. & Dahlborg, U. (2002). Synthesis of Cu47Ti34Zr11Ni8 bulk metallic glass by warm extrusion of gas atomized powders. *Journal of Materials Research,* Vol. 17, No. 1, (January 2002), pp. 186-198, ISSN 0884-2914

Spassov, T. & Koster, U. (1993). Grain-growth in nanocrystalline zirconium-based alloys. *Journal of Materials Science,* Vol. 28, No. 10, (May 1993), pp. 2789-2794, ISSN 0022-2461

Suryanarayana, C. & Inoue, A. (2011). *Bulk metallic glasses*. CRC Press, ISBN 978-1-4200-8597-6, Boca Raton London New York

Suzuki, K.; Kataoka, N.; Inoue, A.; Makino, A. & Masumoto, T. (1990). High saturation magnetization and soft magnetic-properties of bcc Fe-Zr-B alloys with ultrafine grain-structure. *Materials Transactions JIM,* Vol. 31, No. 8, (August 1990), pp. 743-746, ISSN 0916-1821

Suzuki, K.; Makino, A.; Inoue, A. & Masumoto, T. (1993). Low core losses of nanocrystalline Fe-M-B (M=Zr, Hf, or Nb) alloys. *Journal of Applied Physics,* Vol. 74, No. 5, (September 1993), pp. 3316-3322, ISSN 0021-8979

Takeuchi, A.; Inoue, A. & Makino, A. (1997). Improvement of hard magnetic properties of Fe90Nd7B3 alloys by two-stage crystallization treatment. *Materials Science and Engineering A,* Vol. 226-228, No. 1-2, (June 1997), pp. 636-640, ISSN 0921-5093

Turnbull, D. (1981). Metastable structures in metallurgy. *Metallurgical Transactions B,* Vol. 12, No. 2, (June 1981), pp. 217-230, ISSN 0360-2141

Volkert, C.A. & Spaepen, F. (1989). Crossover relaxation of the viscosity of Pd40Ni40P19Si1 near the glass-transition. *Acta Metallurgica,* Vol. 37, No. 5, (May 1989), pp. 1355-1362, ISSN 0001-6160

Wang, W.H.; Dong, C. & Shek, C.H. (2004). Bulk metallic glasses. *Materials Science and Engineering R,* Vol. 44, No. 2-3, (June 2004), pp. 45-89, ISSN 0927-796X

Wang, W.H. (2009). Bulk metallic glasses with functional physical properties. *Advanced Materials,* Vol. 21, No. 45, (December 2009), pp. 4524-4544, ISSN 0935-9648

Willard, M.A.; Laughlin, D.E.; McHenry, M.E.; Thoma, D.; Sickafus, K.; Cross, J.O. & Harris, V.G. (1998). Structure and magnetic properties of (Fe0.5Co0.5)(88)Zr7B4Cu1 nanocrystalline alloys. *Journal of Applied Physics,* Vol. 84, No. 12, (December 1998), pp. 6773-6777, ISSN 0021-8979

Withanawasam, L.; Murphy, A.S.; Hadjipanayis, G.C. & Krause, R.F. (1994). Nanocomposite R(2)Fe(14)B/Fe exchange-coupled magnets. *Journal of Applied Physics,* Vol. 76, No. 10, (November 1994), pp. 7065-7067, ISSN 0021-8979

Xu, J.; Ramamurty, U. & Ma, E. (2010). The fracture toughness of bulk metallic glasses. *JOM,* Vol. 62, No. 4, (April 2000), pp. 10-18, ISSN 1047-4838

Yang, C.; Wang, W.K.; Liu, R.P.; Zhan, Z.J.; Sun, L.L.; Zhang, J.; Jiang, J.Z.; Yang, L. & Lathe, C. (2006). Crystallization of Zr41Ti14Cu12.5Ni10Be22.5 bulk metallic glass under high pressure examined by in situ synchrotron radiation x-ray diffraction. *Journal of Applied Physics,* Vol. 99, No. 2, (January 2006), pp. 023525, ISSN 0021-8979

Yao, K.F. & Ruan, F. (2005). Pd-Si binary bulk metallic glass prepared at low cooling rate. *Chinese Physics Letters,* Vol. 22, No. 6, (June 2005), pp. 1481-1483, ISSN 0256-307X

Ye, F. & Lu, K. (1999). Pressure effect on crystallization kinetics of an Al-La-Ni amorphous alloy. *Acta Materialia,* Vol. 47, No. 8, (June 1999), pp. 2449-2454, ISSN 1359-6454

Zhang, L.C. & Xu, J. (2002). Formation of glassy Ti50Cu20Ni24Si4B2 alloy by high-energy ball milling. *Materials Letters,* Vol. 56, No. 5, (November 2002), pp. 615-619, ISSN 0167-577X

Zhang, L.C.; Xu, J. & Ma, E. (2002). Mechanically alloyed amorphous Ti50(Cu0.45Ni0.55)(44-x)AlxSi4B2 alloys with supercooled liquid region. *Journal of Materials Research,* Vol. 17, No. 7, (July 2002), pp. 1743-1749, ISSN 0884-2914

Zhang, L.C.; Shen, Z.Q. & Xu, J. (2003). Glass formation in a (Ti,Zr,Hf)-(Cu,Ni,Ag)-Al high-order alloy system by mechanical alloying. *Journal of Materials Research,* Vol. 18, No. 9, (September 2003), pp. 2141-2149, ISSN 0884-2914

Zhang, L.C. & Xu, J. (2004). Glass-forming ability of melt-spun multicomponent (Ti, Zr, Hf)-(Cu, Ni, Co)-Al alloys with equiatomic substitution. *Journal of Non-Crystalline Solids,* Vol. 347, No. 1-3, (November 2004), pp. 166-172, ISSN 0022-3093

Zhang, L.C.; Shen, Z.Q. & Xu, J. (2005a). Mechanically milling-induced amorphization in Sn-containing Ti-based multicomponent alloy systems. *Materials Science and Engineering A,* Vol. 394, No. 1-2, (March 2005), pp. 204-209, ISSN 0921-5093

Zhang, L.C.; Shen, Z.Q. & Xu, J. (2005b). Thermal stability of mechanically alloyed boride/Ti50Cu18Ni22Al4Sn6 glassy alloy composites. *Journal of Non-Crystalline Solids,* Vol. 351, No. 27-29, (August 2005), pp. 2277-2286, ISSN 0022-3093

Zhang, L.C.; Xu, J. & Eckert, J. (2006a). Thermal stability and crystallization kinetics of mechanically alloyed TiC/Ti-based metallic glass matrix composite. *Journal of Applied Physics,* Vol. 100, No. 3, (August 2006), pp. 033514, ISSN 0021-8979

Zhang, L.C.; Xu, J. & Ma, E. (2006b). Consolidation and properties of ball-milled Ti50Cu18Ni22Al4Sn6 glassy alloy by equal channel angular extrusion. *Materials Science and Engineering A,* Vol. 434, No. 1-2, (October 2006), pp. 280-288, ISSN 0921-5093

Zhang, L.C.; Calin, M.; Branzei, M.; Schultz, L. & Eckert, J. (2007a). Phase stability and consolidation of glassy/nanostructured Al85Ni9Nd4Co2 alloys. *Journal of Materials Research,* Vol. 22, No. 5, (May 2007), pp. 1145-1155, ISSN 0884-2914

Zhang, L.C.; Kim, K.B.; Yu, P.; Zhang, W.Y.; Kunz, U. & Eckert, J. (2007b). Amorphization in mechanically alloyed (Ti, Zr, Nb)-(Cu, Ni)-Al equiatomic alloys. *Journal of Alloys and Compounds,* Vol. 428, No. 1-2, (January 2007), pp. 157-163, ISSN 0925-8388

Zhang, T.; Inoue, A. & Masumoto, T. (1991). Amorphous Zr-Al-TM (TM = Co, Ni, Cu) alloys with significant supercooled liquid region of over 100 K. *Materials Transactions JIM,* Vol. 32, No. 11, (November 1991), pp. 1005-1010, ISSN 0916-1821

Zhong, Z.C.; Jiang, X.Y. & Greer, A.L. (1997). Nanocrystallization in Al-based amorphous alloys. *Philosophical Magazine B,* Vol. 76, No. 4, (October 1997), pp. 505-510, ISSN 0141-8637

Zhuang, Y.X.; Jiang, J.Z.; Zhou, T.J.; Rasmussen, H.; Gerward, L.; Mezouar, M.; Crichton, W. & Inoue, A. (2000). Pressure effects on Al89La6Ni5 amorphous alloy crystallization. *Applied Physics Letters,* Vol. 77, No. 25, (December 2000), pp. 4133-4135, ISSN 0003-6951

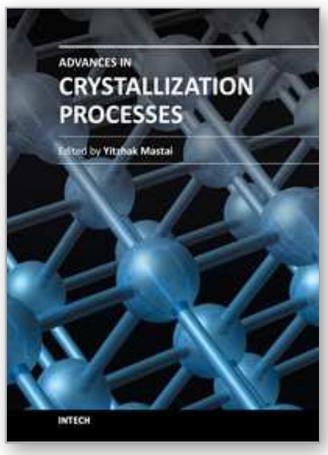

Advances in Crystallization Processes

Edited by Dr. Yitzhak Mastai

ISBN 978-953-51-0581-7
Hard cover, 648 pages
Publisher InTech
Published online 27, April, 2012
Published in print edition April, 2012

Crystallization is used at some stage in nearly all process industries as a method of production, purification or recovery of solid materials. In recent years, a number of new applications have also come to rely on crystallization processes such as the crystallization of nano and amorphous materials. The articles for this book have been contributed by the most respected researchers in this area and cover the frontier areas of research and developments in crystallization processes. Divided into five parts this book provides the latest research developments in many aspects of crystallization including: chiral crystallization, crystallization of nanomaterials and the crystallization of amorphous and glassy materials. This book is of interest to both fundamental research and also to practicing scientists and will prove invaluable to all chemical engineers and industrial chemists in the process industries as well as crystallization workers and students in industry and academia.

InTech Europe
University Campus STeP Ri
Slavka Krautzeka 83/A
51000 Rijeka, Croatia
Phone: +385 (51) 770 447
Fax: +385 (51) 686 166
www.intechopen.com

InTech China
Unit 405, Office Block, Hotel Equatorial Shanghai
No.65, Yan An Road (West), Shanghai, 200040, China
中国上海市延安西路65号上海国际贵都大饭店办公楼405单元
Phone: +86-21-62489820
Fax: +86-21-62489821

IntechOpen